Available online at www.sciencedirect.com

ScienceDirect

Progress in Crystal Growth and Characterization of Materials 62 (2016) 227–251

www.elsevier.com/locate/pcrysgrow

Review

# Three study cases of growth morphology in minerals: Halite, calcite and gypsum

Dino Aquilano [a], Fermín Otálora [b], Linda Pastero [a], Juan Manuel García-Ruiz [b,*]

[a] *Dipartimento di Scienze della Terra, Università degli Studi di Torino, via V. Caluso 35, 10125, Torino, Italy*

[b] *Laboratorio de Estudios Cristalográficos, Instituto Andaluz de Ciencias de la Tierra, CSIC-Universidad de Granada, Armilla, Granada, Spain*

Available online 30 May 2016

**Abstract**

Beyond fundamental aspects of crystal growth and morphology, the growth of minerals is a challenging subject because in most cases we face a problem with unknown growth conditions. Actually, in the field of geological studies, we have to decipher the growth conditions of a crystal using the information contained in the very crystal. One of these characteristics of crystals that contain information about their growth is their morphology and time evolution. In this article, we introduce the subject of crystal morphology by using three important minerals, calcite, halite and gypsum, as three didactic case studies to illustrate the application of the current knowledge in the field.



*Keywords:* crystal growth; morphology; crystal growth; calcite; halite; gypsum

## 1. Introduction

Minerals are, by a vast majority, natural crystals. They grew under unknown conditions that we must reveal with the information contained in their own physical and chemical features. Among these features, their morphology and the surface topography of their faces are key to understand their growth mechanisms. This is why the study of crystal morphology is so important for mineral growth and the reason why mineralogists were the first to contribute the main ideas for the understanding of the shape of crystals. One of these ideas is the differentiation between the morphology derived from the crystal structure – termed structural morphology – and the actual morphology of the crystals as found in nature – termed growth morphology. The structural morphology is drawn by the faces that a crystal will develop considering only the structural and bonding properties of the different khl planes of its structure. In some cases, the structural morphology has been associated with the "equilibrium morphology", which is the morphology of a crystal in equilibrium with the solution, gas or melt. However, by definition, this equilibrium morphology should include the interaction of the crystal faces with the mother phase and therefore do not necessarily fit the structural morphology. The third and most important type of morphology is the termed growth morphology, which is the morphology of the crystals that result from the interaction of the crystal surfaces with the solution, melt or gas, from which a crystal grew, including not only their chemical composition, but also the values of the physical parameters relevant to crystallization, such as temperature, supersaturation, pressure, fluid dynamics and the presence of impurities in the mother phase.

* Corresponding author. Laboratorio de Estudios Cristalográficos, Instituto Andaluz de Ciencias de la Tierra, CSIC-Universidad de Granada, Armilla, Granada, Spain. Tel.: +34 958 230000 (ext 190201); fax: +34 958 552620.

*E-mail address:* juanmanuel.garcia@csic.es (J.M. García-Ruiz).

http://dx.doi.org/10.1016/j.pcrysgrow.2016.04.012

By definition, the growth of actual crystal is a function of time. The conditions under which minerals grow in most cases vary from their nucleation to the cessation of growth. Therefore, in very few cases, the crystals kept the same growth faces and the same relative development of faces. Actually, even the dominant growth mechanism may change during the growth history. The morphology of the mineral we found in the field is the one frozen at the end of the growth process. But the growth history of the crystal can be studied from their cross sections. To extract information from all these internal features it is important to understand what controls the morphology of a growing crystal.

There are several reviews and books that explain the different types of morphology and fundamental aspects of crystal morphology, which are referenced in a separate list of monographs at the end of the manuscript. However, there are very few studies where the different theoretical aspects are explained in detail to specify real cases of crystal growth. Therefore, for this tutorial review, rather than to offer again a theoretical treatment of crystal morphology, we have preferred to present in detail the morphological characterization of three minerals that are of enormous interest because their natural abundance, their industrial interest and their challenge to understand their growth morphology. We have selected the case of halite, NaCl, calcite ($CaCO_3$) and gypsum ($CaSO_4{\cdot}2H_2O$). All the three cases deal with single or twinned crystal. For a treatment of growth pattern the reader is referred to a recent review and the references therein (García-Ruiz and Otálora, 2015).

## 2. Halite (NaCl, space group Fm3m)

### *2.1. Geological occurrence and industrial importance*

Halite, chemically sodium chloride (NaCl), is the mineral commonly known as salt (Fig. 1). In geology, a rock composed primarily of halite is known as "rock salt." Geologically speaking, halite is an evaporitic mineral that forms by evaporation in arid climates. Large deposits of salts have their origin in the desiccation of seas, like in the so-called Messinian crisis when the influx of water from the Atlantic to the Mediterranean ceased or was so small that did not match the flow due to evaporation. Contemporaneously, inland lakes such as the Great Salt Lake (U.S.) and the Dead Sea between Jordan and Israel are also locations where halite is forming today.

Halite has weak hardness (Mohs scale 3) and, under quite moderate pressure, rock salt flows much like ice. The dry Zagros Mountains (Iran) feature some notable salt glaciers. So does the continental slope of the Gulf of Mexico, where there's so much buried salt that it can emerge faster than the sea dissolving it. Besides flowing downward as glaciers, salt can rise upward into overlying rock beds as buoyant, balloon-shaped bodies (salt diapir) which are widespread in the south-central United States, in the Gulf of Mexico; large fields of salt domes have also been discovered in Angola, Brazil, Canada, Gabon, Germany, Iran and Iraq. Rocksalt is an impermeable rock that has the ability to seal fractures that might develop within it. This property of the salt rocks can make them important sites for underground storage or underground disposal of hazardous waste, including nuclear waste. Man-made caverns in salt domes have been used as repositories for oil field drilling waste and other types of hazardous waste in the United States and other countries.

Fig. 1. The cubic habit of a natural sample of Halite (Wieliczka, Poland). Photo: J.M. García-Ruiz.

Beyond their importance in Earth Sciences, sodium chloride is also a very important industrial material. Until the technological revolution, salt was considered the most important mineral resource because of its importance as a food preservative. Even today, salt is a precious material in arid or isolated regions of the planet because it is vital in our diet as well as in the diet of animals. In first world countries, crystal morphology, texture and composition of halite are subjects of continuous investigation. Today, it is also very important that the use of halite in the chloralkali industry as well as in de-icing for winter road maintenance, and as the main component in desalination factories. In addition to these applications, research on halite crystallization is driven also because halite is a byproduct of many chemical engineering and natural processes that have a tendency to cake, i.e., to form large agglomerates of material. It is therefore pertinent to develop methods of how to engineer the NaCl crystals to reduce or remove caking.

### 2.2. Crystal structure and growth morphology of natural halite

Halite crystallizes in the cubic system, with a face centered lattice, f.c.c. (space group Fm3m), its lattice parameter being $a_0 = 5.64$Å. Halite, along with all the f.c.c. alkali halides, exhibits a peculiar feature: while the ideal surface structure of both the cube {100} (Fig. 2a) and the rhomb-dodecahedron {110} (Fig. 2b,c) are not polar since the lattice planes of indices h00 and hh0 are electrically neutral, the ideal octahedron {111} faces (Fig. 2d,e) are unstable since they are electrostatically polar, even if the structure of the crystal bulk is centersymmetric, for positively and negatively charged lattice planes alternate along the four equivalent <111 > directions.

This implies that when halite grows from vapor phase, the only form present is the cube, as it was found two centuries ago, when analyzing the sublimation products of blast furnaces. However, when growing from pure aqueous solution, the sole {111} octahedron truncates the cube when the solution supersaturation (β) exceeds a critical value related to the specific crystal species among all the alkali halides having f.c.c. structure, as proved in the Sixties by Bienfait et al. [1].

The morphology of natural halite is largely dominated by the cube {100}; the {110} and {111} forms are seldom present. When crystals grow by evaporation from aqueous solution the perfection of the cube faces is usually lost; owing to the high values of the supersaturation, hopper shaped {100} faces appear along with dendritic branches developing in the <111 > directions. This is the main reason of the halite tendency to cake. Hence, the best way to face this problem is to search for additives able to favor the appearance of the {111} form, thus avoiding the morphological instability such as the "hazardous" dendritic growth.

### 2.3. Experimental observations on the habit changes in NaCl

Historically, the first example of a habit modifier for NaCl was discovered, in 1783, by Romé d'Isle who reported the habit change from {100} → {100} + {111} in the presence of urea [2]. This has led to the discovery of other NaCl habit modifiers such as formamide, cadmium chloride, ferrocyanide ions and, recently, polymeric additives. Gille and Spangeberg [3] found {100} →{111} change by evaporating aqueous NaCl solutions in the presence of formamide. A wider research was done in the Bienfait et al.'s group [1]: the stability domains of {100} and {111} forms was identified as a function of two parameters: the initial supersaturation of the solution with respect to NaCl and the formamide concentration in solution (morphodrome). An interpretation was attempted by considering that both urea and formamide, due to their similar steric hindrance, do occupy the vacant sites on the octopolar reconstructed {111} form, where the surface electric field reaches its highest value. The stability of the {111} form should further increase (with respect to that obtained in pure aqueous solution) since the dipole moment of urea and formamide is definitely higher than that of the water molecule.

Hartman [4] gave an original interpretation to the {100}→{100} + {111} habit change, occurring when NaCl grows from Cd-doped aqueous solution. Starting from the Royer's hypothesis about the epitaxy [5], he imagined that a 2D-(00.1) layer of the rhombohedral $CdCl_2$ can form a good epitaxy with the (111)-NaCl face, following the coincidences between the triangular 2D lattices of both crystal faces. According to this model, the $CdCl_2$ impurity is adsorbed as an ordered phase and: (i) on one hand, it lowers the specific surface energy of the (111) face of the NaCl crystal, which probably enters the equilibrium shape of the crystal in the doped solution;

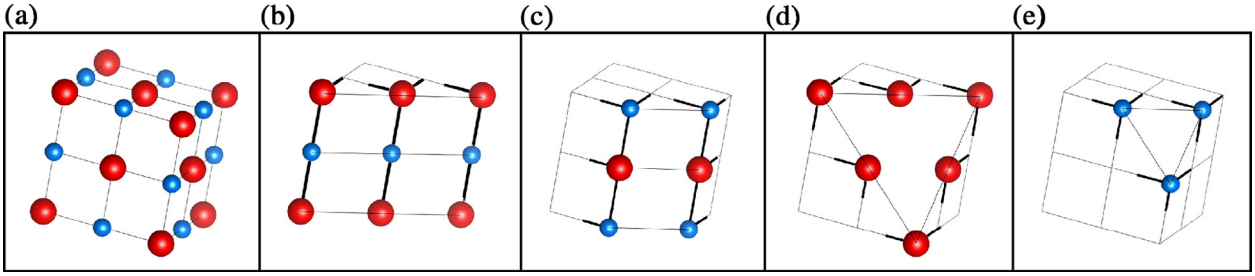


Fig. 2. Ideal surface structure of: (a) the cube {100}; (b, c) the rhomb-dodecahedron {110}; (d, e) the octahedron {111}. Bonds are highlighted. One can see that the contiguous lattice planes, parallel to the {100} and {110} faces, are electrically neutral; on the contrary, the lattice planes parallel to the {111} form are alternately populated by positive and negative charges. (For interpretation of the references to colour in this figure legend, the reader is referred to the web version of this article.)

(ii) on the other hand, the growth kinetics of the (111) face decreases as well, since the percentage of fresh (111) NaCl surface is surely reduced by the $CdCl_2$ adsorbed 2D islands.

Later on, Boistelle and Simon [6] observed a 3D epitaxy between the {111}-NaCl faces and the {00.1} faces of a rhombohedral mixed salt of composition $CdCl_2{\cdot}2\,NaCl{\cdot}3H_2O$, which can form in Cd-doped NaCl supersaturated aqueous solutions. Then, they were able to show as well that a 2D epitaxial coincidence between the {00.1} faces of this mixed salt results to be even better than that calculated by Hartman. Accordingly, the idea of the habit change due to the action of a specific impurity adsorbed as an epitaxial layer is reinforced.

Low concentration of the anion $Fe(CN)_6^{4-}$ is commonly used to prevent or control NaCl nucleation and growth in weathered rocks and construction materials (e.g., stones and concrete), and to avoid salt crystallization damage due to NaCl sub-fluorescence growth in porous stones. Alternatively it is used as an anticaking agent for road deicing or as an additive for the food industry. Coming back to formamide, this additive is not known for its efficiency as a NaCl habit modifier, at very low or low concentrations, or for its industrial applications. Nevertheless, its ability to progressively modify the NaCl habit when its concentration in aqueous solutions varies from 0 to 100%, makes it of relevant interest to investigate, from the fundamental point of view, the growth mechanisms in the system: formamide–water–NaCl crystal (Fig. 3).

Recently, Radenović et al. [8a,8b] confirmed the above-mentioned observations by evaporating at room temperature NaCl aqueous solutions containing up to 30% of formamide and outlined that the presence of formamide enhances the quality of NaCl crystals, since the number of fluid inclusions sharply decreases with respect to those found after growth from pure aqueous solutions. Moreover, through a surface X-ray diffraction (SXRD) determination of the {111} NaCl–liquid interface structure and using ultrathin water or formamide adsorbed liquid layers, they ascertained that: (i) the crystal surface is smooth and is not reconstructed; (ii) small differences in surface structure between the water or formamide liquid layers, which nevertheless lead to dramatic differences in crystal morphology. From SXRD, they determined as well that the {111} surface is $Na^+$ terminated for both environmental conditions and that 0.25–0.5 of a monolayer of laterally disordered $Cl^-$ ions is located on top of a fully ordered $Na^+$ crystal surface with occupancy 0.75–1.0. Accordingly, the polar surface is stabilized through the formation of an electrochemical double layer. A further consideration has been proposed to detail the influence of formamide on the NaCl morphological change: they noticed that for alkali halide crystals grown from saturated formamide solutions, the appearance of the {111} form is strictly related to their unit cell size [8b]. Very recently, they also discovered [8c] that a polymer additive containing an amide functional group induces the formation of the {111} faces on NaCl crystals with a one to two orders of magnitude stronger effect than the corresponding monomer; this is a consequence of the enhanced bonding of the polymer compared with the monomer. However, if the polymer does not contain a suitable active functional group for habit modification, the anticaking effect is nil and the crystal habit shows only the cube (Fig. 4).

As mentioned above, during the last four decades many contributions concerned mainly the nature and occurrence of the octahedron (both from vapor and solution growth) were extensively discussed from the experimental and theoretical point of view. Recently, the existence of the octahedron in aqueous solution has been experimentally excluded, except in the presence of critical amounts of specific impurities. This means that a con-

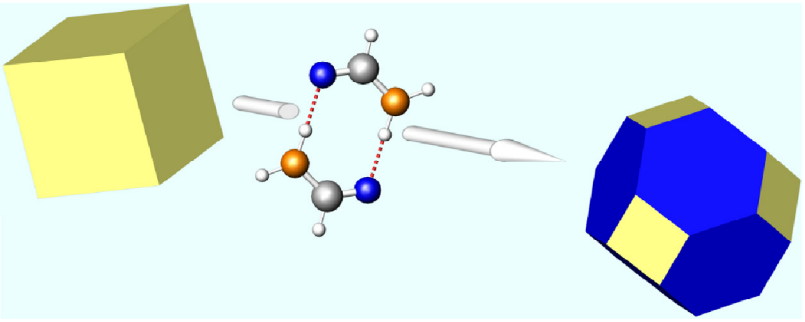

Fig. 3. Habit change occurring on NaCl crystals when formamide is added during growth from aqueous solution. Reprinted with permission from Pastero et al. [7]. Copyright © 2012, ACS. (For interpretation of the references to colour in this figure legend, the reader is referred to the web version of this article.)

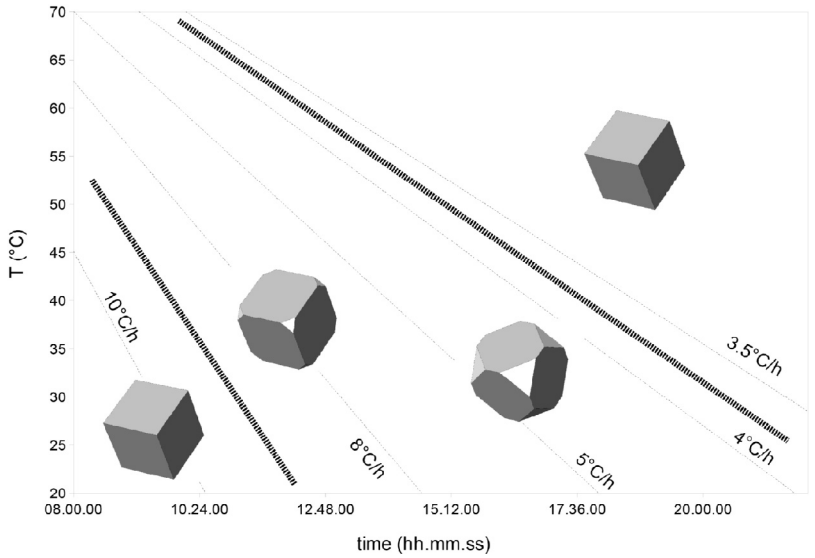


Fig. 4. Morphology of NaCl crystals grown from pure aqueous solutions in a closed system according to different temperature gradients (T vs time). Initial $T_{sat}$ and final $T_{cryst}$ are 95 and −5 °C, respectively. Only {100} form is observed when the gradient is lower than 3.5 °C/h; {100} and {111} forms coexist when the gradient varies in between 3.5 and 8 °C/h; for higher gradients no crystals have been observed. The mid-line corresponds to the slope of 4 °C/h. Second generation crystals are composed by {100} + {111} forms, while in larger crystals (first generation) only {100} form survives to the kinetic competition. Adapted from Aquilano et al. [9]. Courtesy by Elsevier.

troversy has been generated in the scientific community about the morphology of a structurally simple but very important series of minerals such as the f.c.c. alkali halides.

### 2.4. Explaining the NaCl morphology change {100} → {110} + {111}

For the sake of clarity, we will recollect the fundamentals to explain the well-tested experimental observation following two different paths. First, we will search the theoretical equilibrium shape of halite, having kept in mind that the *equilibrium shape of a crystal is unique*, according to the Curie-Gibbs condition [10], which has to be fulfilled for a crystal, at thermodynamic equilibrium:

$$\Phi_i = \sum_{i=1}^{n} \gamma_i S_i = \text{minimum}; \delta V = 0 \quad (1a)$$

where $\Phi_i$, the total surface energy of a crystal limited by *i* faces (each having surface area, $S_i$, and specific surface energy, $\gamma_i$) should be minimal, while the crystal volume V does not vary.

The equation system (1a) has a simple solution:

$$\frac{\gamma_1}{h_1} = \frac{\gamma_2}{h_2} = \cdots = \frac{\gamma_i}{h_i} = \text{constant} \quad (1b)$$

where the term $h_i$ is proportional to the distance (in the 3D space) from the *i* face to a arbitrarily fixed point. This continuous proportion shows that higher the $\gamma_i$ value, the higher the distance $h_i$ : accordingly, the equilibrium shape will be a convex polyhedron limited by the faces with lowest surface energy values. Equation (1b) is nothing else than the Wulff's theorem and the corresponding polyhedron representing the equilibrium shape is called the Wulff's plot [11]. Then, the equilibrium shape only depends on the specific surface energies ($\gamma_i$), i.e. from the thermodynamic properties of the interface crystal/mother phase.

Secondly, we will attempt a reasonable interpretation of the *growth shapes, which are not unique,* since they depend on the character of the crystal forms, on kinetic factors affecting the mother phase, on fluid dynamics and on the density and quality of defects arising in the crystal bulk.

#### 2.4.1. NaCl crystallography

Stranski [12a], Bertaut [12b] and Hartman [12c] theoretically proved that the ideal {111} surfaces of the NaCl-like structures cannot be stable in the presence of their own vapor. Fig. 2 shows that these ideal surfaces are made either by a 2D array of positive ($Na^+$) or negative ($Cl^-$) charges. In other words, the two outmost surface layers can be seen as 2D arrays of iso-oriented electric dipoles. This make unstable the surface, since the lattice sum representing the potential energy of an infinite slab of thick-

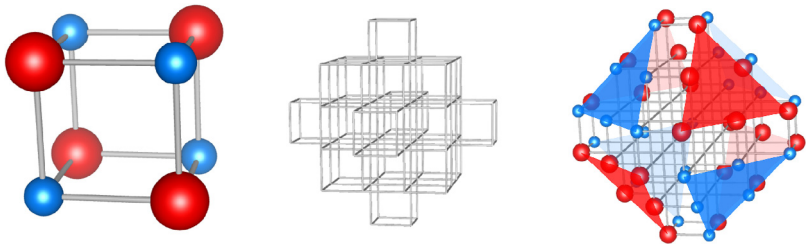

Fig. 5. (Left) NaCl octopole; (center) NaCl octahedron built by octopoles; (right) view of the outmost layer of the {111} form built by octopoles. Surface symmetry is that of two complementary tetrahedra showing opposite charges on their surfaces. (For interpretation of the references to colour in this figure legend, the reader is referred to the web version of this article.)

ness equal to $n \times d_{111}$ does not converge near the outermost 111 planes, even if $n$ is finite. On the contrary, finite ($7 \times 7$ nm$^2$) triangular NaCl (111) islands having three-layered Na–Cl–Na bulk structure are stable, as it has been observed in the aluminum/NaCl vapor-phase epitaxy [13]. An opposite situation obtains, for the{100} form, where each 100 plane is electrically neutral and hence the potential energy near the {100} surface maintains balanced even for infinite slab extension. Among the ways proposed to cancel out the dipole moment normal to the ideal {111} form, we will confine our attention to the stable {111} surfaces as reconstructed by octopoles, which is by far the most reasonable model [14], since it is the only one for which an experimental evidence was found for the vapor growth [15] and also because this way of reconstructing respects the symmetry of the surface point group. Octopoles are electrically neutral objects lacking dipole moment (Fig. 5, left), which can be imagined to build a crystal showing both {100} and {111} forms that, in turn, can be generated by different stacking of octopoles along the main directions <100 > . Hence, the reconstructed octahedron does not exhibit dipole moment on its surfaces (Fig. 5, center); moreover, its outermost layer contains only 25% of the available lattice sites, while the two layers below contain 75% and 100% of the sites. One should also consider that such a reconstruction changes the resulting surface symmetry: in fact, if the (111) face is Na-terminated, the ($\bar{1}\bar{1}\bar{1}$) face will result Cl-terminated; then, the surface symmetry of the octahedron is broken and is replaced by that of two complementary tetrahedra showing opposite charges on their surfaces (Fig. 5, right). So, the unchanged m3m point group of the crystal bulk will coexist with the "surface" point group $\bar{4}$3m, the two point groups being not incompatible, since $\bar{4}$3m is a subgroup of m3m.

### 2.4.2. *The equilibrium shape of halite*

On this ground and for the first time, all the factors that contribute to determine the specific surface energies, $\gamma_{100}$ and $\gamma_{111}$, for the crystal/vapor interface in the range of the usual experimental temperatures have been considered; a quantum mechanical study was carried out on the bulk and surface structures of both {100} and {111} forms, once their geometries were optimized at the density functional theory (DFT) level [16].

Then, $\gamma$ values were determined as a function of the temperature (both vibrational, bulk and surface, and surface configurational entropies were considered) by implementing a thermodynamic model already elaborated by Kern [17]. The values we calculated at T = 25 °C were $\gamma_{100}^{halite} = 120$ and $\gamma_{111}^{halite} = 310$ erg cm$^{-2}$, respectively. This means that at room temperature and in the presence of its own vapor, the equilibrium shape of halite is only made by the cube, since the geometrical constraint ( $\gamma_{111}^{halite} < \sqrt{3}\gamma_{100}^{halite}$ ) to enter the equilibrium polyhedron is not fulfilled by the {111} form.

Since halite mainly grows from aqueous solution, one has to investigate if its equilibrium shape could change when water adsorption is considered, i.e. we must evaluate both $\gamma_{NaCl-solution}^{100}$ and $\gamma_{NaCl-solution}^{111}$. To this end, we used:

(i) $\gamma_{sat.sol-vap}$ , the surface energy between the NaCl saturated solution and the surrounding water vapor, which is equal to 82 erg cm$^{-2}$, at the pressure of 1 atm and at 25 °C [18,19],
(ii) $\gamma_{water-vap}$ , the surface energy between liquid water and its vapor, equal to 72 erg cm$^{-2}$.
(iii) $\gamma_{NaCl-solution}^{100}$ , the specific surface energy between the {100} NaCl form and its saturated solution, at T = 25 °C, equal to 63 erg cm$^{-2}$ [19].

It should be remembered as well that the same authors [19] obtained $\gamma_{NaCl}^{100} = 114$ erg cm$^{-2}$, which agrees fairly well with the value $\gamma_{100}^{halite} = 120$ erg cm$^{-2}$ calculated above. Thus, one can reasonably assume, for the equilibrium crystal/its vapor, the mean value $\gamma_{NaCl-vapor}^{100} = 117$ erg cm$^{-2}$ .

When two condensed phases (e.g. a crystal and a liquid) have a common interface, in the presence of a common vapor phase, the interfacial energy $\gamma_{solid/liquid}$ is ruled by the Dupré's relation [16, pg. 90]:

$$\gamma_{solid/liquid} = \gamma_{solid/vapor} + \gamma_{liquid/vapor} - \beta^{adhesion}_{solid/liquid} \quad (2a)$$

By applying this formula to the {100} NaCl form immersed in its own saturated solution, at T = 25 °C, it follows:

$$\gamma^{100}_{NaCl-solution} = \gamma^{100}_{NaCl-vapor} + \gamma_{solution/vapor} - \beta^{adh}_{NaCl(100)/solution} \quad (2b)$$

where $\beta^{adh}_{NaCl(100)/solution}$ represents the specific adhesion energy between a (100) NaCl face and the surrounding solution at equilibrium; from the just quoted values one finds the calculated value: $\beta^{adh}_{NaCl(100)/solution} = 136\ \text{erg cm}^{-2}$. When dealing with the contact between two condensed phases, a key question arises about the reliability of the calculated energy values: is it reasonable that the calculated value we found is $\beta^{adh}_{NaCl(100)/solution}$? From the general Young's and Dupré's relations one deduces that the adhesion energy, between a solid and the 3D-liquid surrounding it, must respect the constraint: $\beta^{adh}_{solid/solution} \le 2\gamma_{solution/vapor}$. In our case, it follows that our calculated value $\beta^{adh}_{NaCl(100)/solution} \le 164\ \text{erg cm}^{-2}$ does fulfil the quoted constraint. From contact angle measurements, von Engelhardt obtained $\beta^{adh}_{NaCl(100)/solution} = 162.3\ \text{erg cm}^{-2}$, which indicates a quasi-perfect wetting [20]. It was measured as well: $\beta^{adh}_{NaCl(111)/solution} = 158.55\ \text{erg cm}^{-2}$. Then, using the value we calculated ($\gamma^{111}_{NaCl-vapor} = 310\ \text{erg cm}^{-2}$), one should obtain $\gamma^{111}_{NaCl-solution} = 233.45\ \text{erg cm}^{-2}$, which is more than twice the value needed in order for the {111} form to enter the equilibrium shape of NaCl in pure aqueous solution.

When summarizing, it is reasonable to assess about the habit of halite:

(i) The{111} halite form cannot belong to the equilibrium polyhedron of the NaCl crystal in pure aqueous solution and hence it cannot appear on the unstable shape of the critical nuclei. It follows that:
(ii) The presence of the octahedron on the shape of the NaCl crystals grown from pure aqueous solution should be only due to a kinetic effect. Accordingly, a mechanism should be found to explain how a face that does not appear on the nucleation shape can appear in the growth shape, as we observed. In other words, one has to imagine some changes in the stability of the steps spreading on the adjacent faces so as to allow the generation of a new surface at their convergence point.

### 2.4.3. *The growth shapes of halite*

Once the ambiguity between equilibrium and growth shapes has been moved, new questions do arise about the mechanism(s) working on the {100} → {100} + {111} NaCl habit change in the presence of formamide.

(i) Is the single adsorbed molecule of the additive, which interacts with peculiar adsorption sites of the growing NaCl crystal, releasing different adsorption energies on the different crystal forms and then differently affecting their advancement rates?
(ii) Otherwise, is the cooperative effect of the adsorbed additive molecules, which are forced to laterally interact among themselves by the crystal field of the substrate, transforming a random adsorption in an ordered (epitaxial) one?
(iii) Finally, are there experimental evidences of an intimate relationships substrate/additive, which allows the additive to enter (either disordered or ordered) in one (more) sector of the growing crystal?

*2.4.3.1. SEM observations and experimental X-ray Powder Diffraction (XRPD) diagrams on NaCl crystals grown in the presence of variable concentrations of formamide.* First, we observed [7] (Fig. 6) the products of our crystallization by a Scanning Electron Microscope, which is an instrument that allows to obtain an "objective information." This is used because the information done by optical microscopy (on the same subjects) can be criticized as "subjective," especially when operating in transmitted light.

Second, XRPD diagrams have been obtained on the just mentioned products of crystallization, focusing the attention on the diffraction peaks corresponding to the $d_{002}$ and $d_{111}$-NaCl spacing (Fig. 7).

From a detailed decomposition of the just mentioned XRPD peaks, it follows that two *well crystallized phases*, NaCl and formamide, *can coexist within the same crystallite, formamide being entered in the {111}-NaCl sectors as $d_{101}$ stacked layers*.

*2.4.3.2. NaCl crystal changes its habit due to the sectorial ordered adsorption of formamide.* Hence, *this habit change of NaCl crystals is not due to the random adsorption of the additive*. On the contrary, *even if the mother solution is unsaturated with respect to formamide, its molecules are forced to organize themselves in 2D-$d_{101}$ layers*

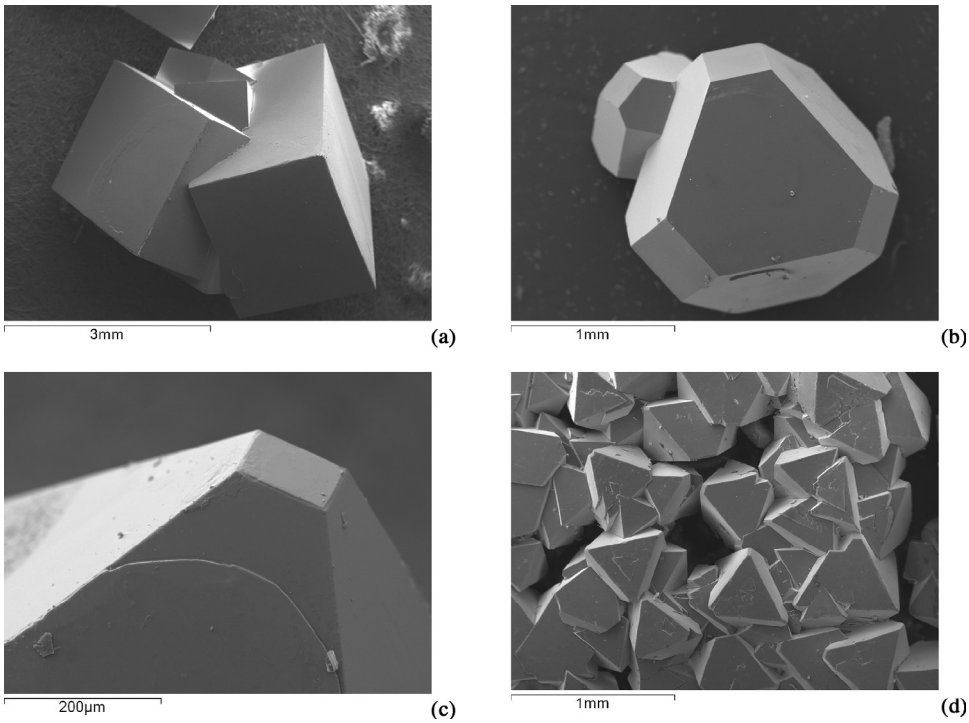


Fig. 6. With reference to Fig. 4, the sketch shows how sensible the result of the habit change of NaCl crystals is when the formamide concentration in the mother aqueous solution varies from 0% (a) to 20% (b,c) and 100% (d). Reprinted with permission from Pastero et al. [7]. Copyright © 2012, ACS.

*by the crystal field imposed by the {111}-NaCl growing substrate, so generating a 2D-epitaxy NaCl/formamide.* The experimental evidence revealed by XRPD has been confirmed either by the calculated geometrical constraints to be fulfilled for the epitaxy to occur, or by the calculation of the interaction energy between a 2D-$d_{101}$ layer of formamide and the {111}-NaCl bulky substrate [7].

At the end of this complex mechanism, an "anomalous mixed crystal" has been generated: *mixed*, because two crystal species occupy the space of a single individual; *anomalous*, because the mixing is not homogeneous but highly inhomogeneous, the absorption behavior within the {100} and {111} growth sectors of NaCl being totally different.

## 3. Calcite ($CaCO_3$)

### 3.1. Geological and industrial aspects

Calcite is the principal rock-forming mineral of limestone (a rock containing at least 50% by weight of calcium carbonate in the form of calcite) and, generally speaking, is the most common carbonate mineral in carbonate sediments and rocks. All limestones contain at least a few percent of terrigenous minerals like quartz, feldspar, and clay minerals. They can also contain authigenic minerals like gypsum, anhydrite, pyrite or siderite.

Carbonate minerals precipitate from supersaturated water by biochemical or direct precipitation processes, and accumulate as marine, terrestrial or shallow

Fig. 7. XRPD spectra obtained at different temperature ($T_{spectrum}$) on NaCl crystals grown at different crystallization temperature ($T_{cr}$) from aqueous solutions saturated at $T_s = 95$ °C, in the presence of different concentration ($C_f$) of formamide. (a) $T_{spectrum} = -5$ °C, $T_{cr} = -5$ °C, $C_f = 20\%$, cooled under a gradient of 20 °C/h. Top: 111-NaCl peak (lower 2θ angle) + 101-formamide peak (higher 2θ angle). Bottom: 002-NaCl peak. (b) $T_{spectrum} = 25$ °C on crystals obtained by evaporation at $T_{cr} = 30$ °C (initial $C_f = 20\%$). Top: Asymmetric 111-NaCl peak (lower 2θ angle). Bottom: 002-NaCl peak. (c) $T_{spectrum} = 25$ °C on crystals obtained by evaporation at $T_{cr} = 30$ °C (initial $C_f = 60\%$). Top: Asymmetric 111-NaCl peak (lower 2θ angle). Bottom: 002-NaCl peak. (d) $T_{spectrum} = 25$ °C on crystals obtained by evaporation at $T_{cr} = 30$ °C from a NaCl pure formamide solution ($C_f = 100\%$). Top: 111-NaCl peak. Bottom: 002-NaCl peak. Adapted from Pastero et al. [7]. Courtesy American Chemical Society.

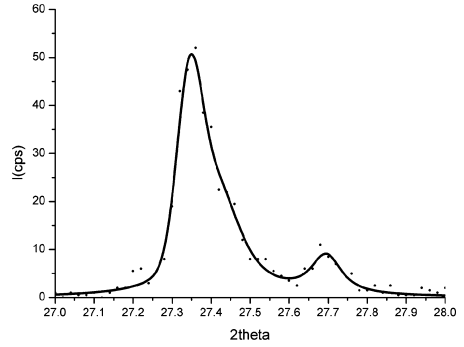
I(cps)
2theta

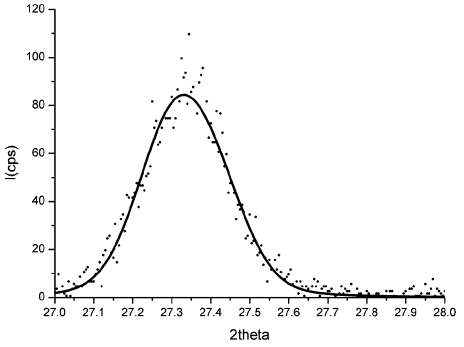
I(cps)
2theta

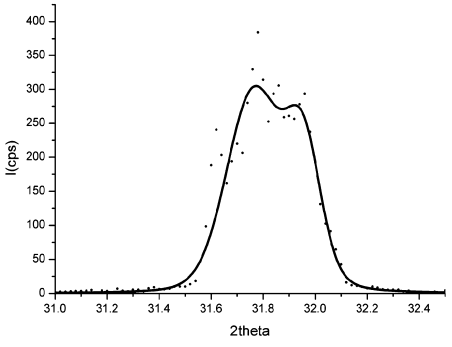
I(cps)
2theta

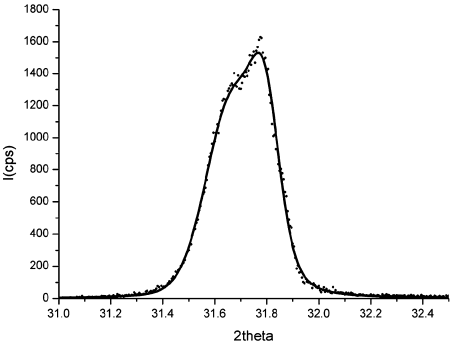
I(cps)
2theta

(a) (b)

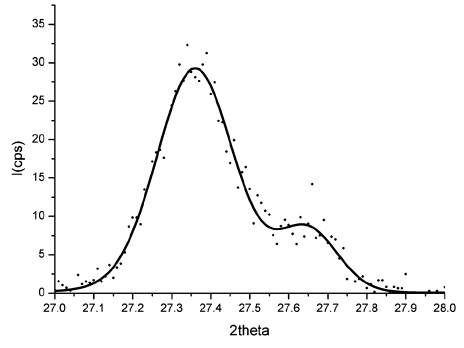
I(cps)
2theta

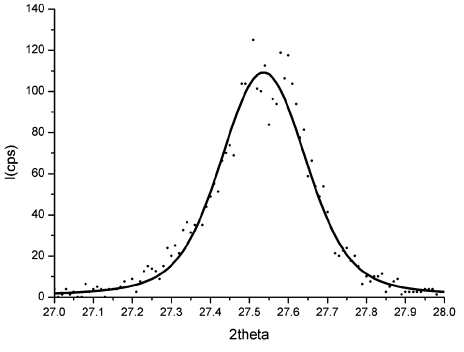
I(cps)
2theta

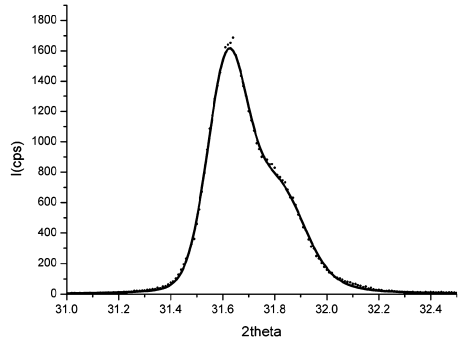
I(cps)
2theta

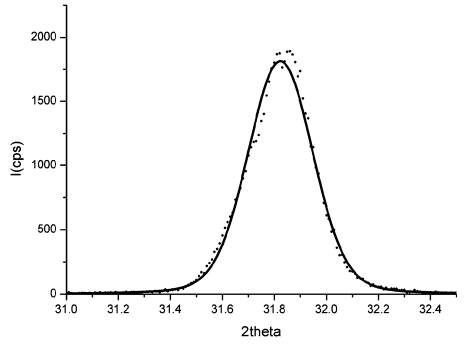
I(cps)
2theta

(c) (d)

tropical seas deposits. Limestone can also form through evaporation. Speleothems and travertine are limestone concretions formed through evaporation. Carbonate rocks represent 1/6 of the global sedimentary mass and can give geological information about the conditions of precipitation, erosion, transportation and deposition. Moreover, the fossil content give information about the environmental conditions during the precipitation. Last, the composition of limestone reflects the composition of waters and its physical-chemical conditions during precipitation. So, studies on carbonate rocks are valuable for the comprehension of many geological and environmental issues as former climates, depth of water, temperature, salinity, proximity to shore, depth of burial and presence of waves or currents.

Limestones can be aquifers with variable water-yielding properties, from confining formations to really productive aquifers. These rocks can act also as hydrocarbons reservoirs due to their porosity and relative permeability that are in turn affected by their composition and geological history and ore deposits for many metals like zinc, mercury, silver and lead. Limestones are an essential mineral commodity. The chemical purity requirements vary by intended use. Depending on its chemical purity, the raw material obtained from carbonate rocks can be used in a large variety of applications: chemical and construction industry, agriculture and environment. For example it can be used as lime (CaO) source for chemicals. It is also applied to soils and water treatment, to metals smelting and as filler in many products (paper, plastic and paint). Limestone is widely used to produce Portland cement and aggregate in concrete and asphalt, or as building stones in building industry.

### 3.2. Crystallography of calcite and similarities with the NaCl structure

The structure of calcite, the stable polymorph of $CaCO_3$ at room temperature and pressure, is rhombohedral (space group $R\bar{3}c$), with lattice parameters and angles: $a_0 = b_0 = 4.969$ Å, $c_0 = 17.06$ Å; $\alpha = \beta = 90°$, $\gamma = 120°$. The strong anisotropy introduced by the planar and triangular $CO_3^{2-}$ ions is not compatible with the higher symmetry of the cubic system; nevertheless, interesting similarities occur between calcite and halite. As a matter of fact: (i) when viewed along its unique axis $A_3$ of maximum symmetry, calcite appears as built by the 00.1 lattice planes populated by alternating positive $Ca^{2+}$ and negative $CO_3^{2-}$ charges, which corresponds to the $Na^+$ and $Cl^-$ 111 layers alternating along the four $A_3$ axes of halite; (ii) the cleavage {10.4} rhombohedron of calcite corresponds to the cleavage {100} cube of halite, the 10.4 lattice planes being populated by an equal number of positive ($2^+$) and negative ($2^-$) charges, in the same way as the 100 planes of NaCl are made by an equal number of positive ($1^+$) and negative ($1^-$) ions.

### 3.3. The equilibrium shape of calcite: from a cliché to the scientific complexity

For a long time, a tale outlasted about the equilibrium shape of calcite. As part of the yet surviving confusion between the equilibrium and growth shape, a diffused conviction has been propagated up to this day, i.e. the {10.4} cleavage rhombohedron plays the double role of both equilibrium and growth shapes of calcite. Frankly speaking, this is too much, even for the most celebrated crystal of the history of crystallography.

Here we will cover the path toward a reliable way of thinking about both equilibrium and growth shapes of calcite.

#### 3.3.1. The importance of the minimum energy profile of the different crystal forms, of the reconstruction of polar surfaces and of the surface relaxation

Heijnen published, in 1985, the first paper that clearly faced the drawbacks encountered when dealing with the polar surfaces found in calcite [21]. Resting on the Hartman's way of thinking (the Periodic Bond Chain analysis, PBC) [22], he found that the steep {01.2} rhombohedron can show two sharply different outmost surface profiles: one,$\{01.2\}_a$, is $Ca^{2+}$ terminated (Fig. 8, right inset), while the other one, $\{01.2\}_b$, is $CO_3^{2-}$ terminated. Moreover, to cancel out the {01.2} surface polarity, he concluded that only one half of the ions lying on the outmost layer (for both calcium and carbonate) has to be taken into account. This complexity does not occur for the cleavage {10.4} rhombohedron, since its surface profile is unique and not affected by polarity (Fig. 8, left inset). To calculate the specific surface energy, $\gamma_{01.2}$, at T = 0 K and without surface relaxation, he adopted for the crystal field a simple electrostatic model made by the elementary charges $Ca^{2+}$ and $C^{+1}O_3^{-1}$ and found, in erg cm$^{-2}$, that $\gamma_{\{10.4\}} = 1089$, $\gamma_{\{01.2\}a} = 3547$ and $\gamma_{\{01.2\}b} = 4351$. Having considered that the $Ca^{2+}$ terminated profile is the most probable and applying the Wulff's plot to the evaluation of the equilibrium shape, it followed that, at 0 K and without relaxation, only the cleavage {10.4} form can enter the equilibrium shape of calcite.

Later on, in the decade 1993–2003, the results obtained by Heijnen were improved by using more suitable potential functions or Hamiltonian to describe the interatomic interactions and by introducing surface relaxation [23]. Nevertheless, due to inappropriate choice

of the surface profiles of the forms investigated ({01.2} {10.0} and {00.1}), the {10.4} form continued to be the only one belonging to equilibrium shape.

Having kept in mind the extremely wide richness of the calcite growth morphology, we attempted to study the most frequently observed growth forms ({10.0}, {21.4}, {01.8}, {10.4}, {01.2}, {10.1}, {00.1} and {11.0}) to verify if they cannot enter the equilibrium polyhedron. Peculiar attention was paid to the forms that need to be reconstructed ({00.1}, {01.2},{10.1}) and to the surface structure of the {00.1} and {01.2} forms, which seems to offer the most suitable interfaces for the preparation of different organic/inorganic monolayer systems in biomineralization processes [24].

To do that, the following procedure has been established:

(i) The Hartman–Perdok analysis [22] was applied to the calcite structure and the character (flat-F, stepped-S, kinked-K) of the faces was identified.
(ii) The surface profiles of the slices, of thickness $d_{hk.l}$, allowed by the extinction rules associated with the space group of calcite, were determined and then the surface reconstructions was performed, when needed.
(iii) Among the possible surface profiles of a given form, those profiles respecting the 3D symmetry of the crystal bulk were carefully considered, to find if they can be associated with the minimum energy of the form.
(iv) The equilibrium polyhedron was calculated, through the Wulff's plot, both at 0 K and at room temperature introducing both configurational and vibrational surface entropies
(v) Surface relaxation was introduced to estimate the differences in the $\gamma_{hk.l}$ values with respect to those obtained with unrelaxed surfaces
(vi) Water adsorption has been evaluated as well.

On the basis of the encouraging results obtained with the {111} form of NaCl, and having considered the strong similarity of the NaCl and calcite structures, we adopted the scheme of the octopole also for determining the surface profiles of the reconstructed {00.1} form of calcite (Fig. 9).

Surprisingly, the {01.2} and {00.1} and {10.0} forms can enter the athermal equilibrium shape of calcite, at variance with all the just quoted works, where the {10.4} form is found to be the only one belonging to the equilibrium morphology. Moreover, when recollecting our results on the reconstructed {01.2} form of calcite and {111} NaCl octahedra, it can be stressed that the bulk crystal symmetry has to be considered if one aims to achieve the self-consistency of the surface reconstruction (Figs. 10 and 11).

At the time being, one can say that an old legend has been finally debunked: if the most reasonable profiles of the calcite forms are taken into account, through the Hartman–Perdok method, and suitable potential functions are used along with temperature effect and surface relaxation, the equilibrium shape is built by two F forms,

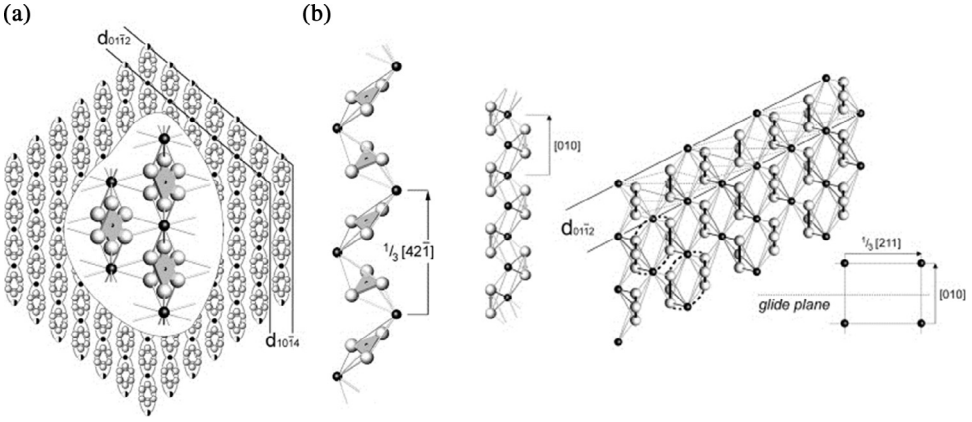


Fig. 8. (Left) The structure of calcite (a) viewed along $[42\bar{1}]$the PBC (b). These periodic bond chains (PBCs) are drawn along with the interconnecting bonds within the slices of $d_{104}$ and $d_{012}$ thickness. The sharp difference between the two slices is due to the fact that Ca ions are shared by contiguous $d_{012}$ slices, while no ion lies on the borders of the $d_{104}$ slice. The half-filled Ca ions (outmost $d_{012}$ layer) indicate that 50% of the Ca ions along the $[42\bar{1}]$ row are missing, as required by the structure of the $[42\bar{1}]$PBC. (Right inset) The structure of calcite viewed along the [010] PBC. Dotted ellipses enclose the helix-shaped [010]PBC (left side): in the resulting outmost Ca layer of the (012) face, 50% of the ions are missing, according to the surface mesh consistent with the bulk symmetry (right side). Adapted from J. Crystal Growth 310, (2008) 706–715. Courtesy by Elsevier, 2008.

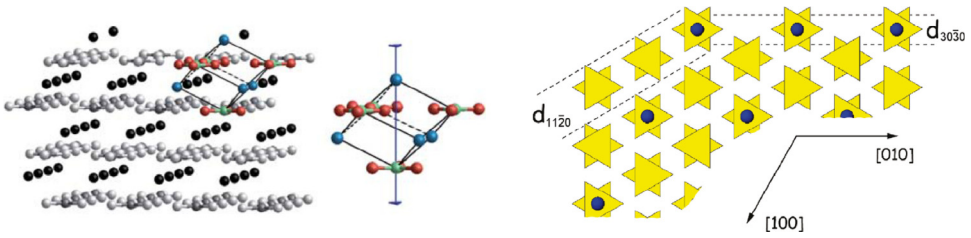


Fig. 9. Ca terminated (00.1) surface profile face of calcite, reconstructed using neutral octopoles. The surface polarity is canceled out by removing 75% of the Ca ions in the outer layer and 25% of the $CO_3$ groups in the underneath one. The octopole (right side), composed by four Ca ions and four $CO_3$ groups stacked along the threefold axis, reproduces the {10.4} cleavage rhombohedron. (For interpretation of the references to colour in this figure legend, the reader is referred to the web version of this article.)

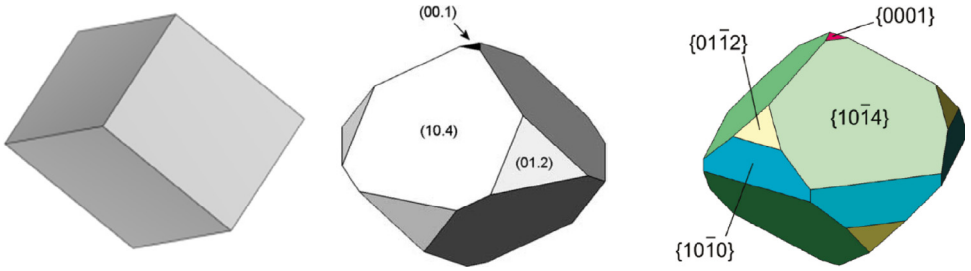


Fig. 10. The evolution of the calculated equilibrium shape of calcite: (left) the "traditional" one is built by the only cleavage rhombohedron; (center) the relaxed one, at 0 K, obtained from the $\gamma_{hkl}$ values using a B3LYP for {10.4} form and Rohl potential function [25] for the other forms. For the reconstructed {01.2} and {00.1} forms the minimum for the $\gamma$ values are obtained when the surface profiles respect the symmetry of the bulk crystal; (right) the final one, at 0 K. when the main {10.4}, {10.0}, {11.0}, {01.8}, {01.2}, {00.1}, and {21.4} forms have been considered. Adapted from Bruno et al. [24i]. Courtesy by RSC. (For interpretation of the references to colour in this figure legend, the reader is referred to the web version of this article.)

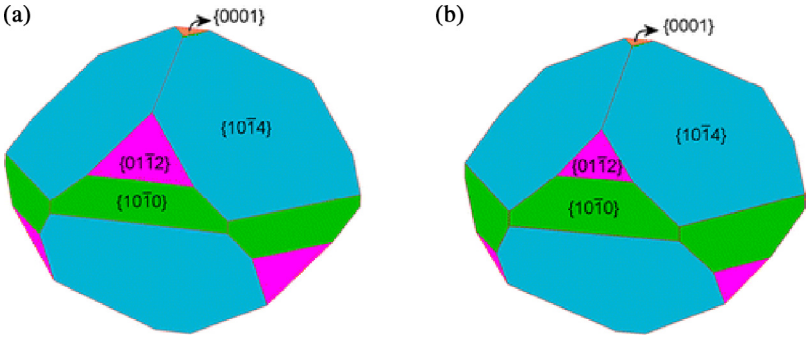


Fig. 11. The comparison between the equilibrium shape of calcite calculated (a) in the presence of water adsorption and (b) in the vacuum shows that the effect of water is fairly homogeneous and moderate. Reprinted with permission from Bruno et al. [24m]. Copyright © 2013, ACS. (For interpretation of the references to colour in this figure legend, the reader is referred to the web version of this article.)

{10.4} and {01.2}, one S form, {10.0}, and a K form, {00.1}. For two out of them, the polar {01.2} and {00.1} forms, a surface reconstruction is needed and, finally, it was found that the $CO_3^{2-}$ terminated surfaces are privileged to build the equilibrium shape of the crystal. All these features have to be necessarily considered when interpreting every experimental results (growth kinetics, epitaxies) where the crystal/mother phase interfaces are involved.

### *3.3.2. Growth shapes of calcite: a complex case study*

As we mentioned above, when dealing with NaCl, while the equilibrium shape of a crystal is unique, for a given T and a surrounding medium, the growth shapes

of a crystal can vary according to the properties (thermodynamic and kinetic) of the mother phase. For that reason, we accounted for an amazing number of combination of growth forms, as comes out from an investigation about *natural calcites* described by Sunagawa [26] and Goldschmidt [27], in his monumental "Atlas der Kristallformen," and concluded that the ranking of the occurrence frequency (%) is: {10.0}(S-46.3), {21.4}(S-38.9), {01.8}(S-37.2), {10.4} (F-35.7), {01.2} (F-24.2), {10.1}(F-23.8), {00.1} (K-17.2), {11.0}(F-14.1), plus other 25 forms with an occurrence frequency comprised between 1% and 6% of the 2500 observed crystals found over the world. Here, within the round brackets, we indicated both the character of the form and the occurrence frequency. At first sight, it is surprising that the three most recurrent forms have stepped (S) character and that the kinked {00.1}K-form should be more important that the flat F-prism {11.0}; however, it is worth remembering that natural crystals usually do not grow from "pure aqueous solutions," and that for calcite, the growth does occur in a wide range of temperature and pressure. For our purpose we will examine some interesting cases of growth morphology.

Historically, the cleavage {10.4} rhombohedron has been the most investigated growth form, owing to its large and shining faces and also because it is the slowest growing form in pure aqueous solutions, due to its strong F character, which allows to produce the best AFM images of growth (or dissolution) surface patterns within a wide range of supersaturations (Fig. 12) [28].

The example of the {00.1} pinacoid permits to show how a kinked face could transform in a flat one (K → F transition), thanks to the modifying effect of a specific impurity present in its mother solution.

As shown in Fig. 13a, when increasing concentrations of $Li^+$ ions are added to an aqueous solution, supersaturated with respect to calcite, the habit of the precipitated calcite crystals dramatically changes from {10.4}→{10.4} + {00.1}→{00.1}; the morphology variation is enhanced by the increasing supersaturation, as drawn in Fig. 13b. It is worth outlining that the solution is unsaturated with respect to a potential precipitation of $Li_2CO_3$; in fact, zabuyelite cannot precipitate. Nevertheless, 2D-epitaxial zabuyelite layers of minimum thickness $d_{002}$ do form on the growing {00.1} calcite faces, the epi-adsorption slowing down the {00.1} advancement rate. The layer growth shown in Fig. 13c is the experimental evidence of the K → F transition in the character of the {00.1} faces.

Fig. 13d shows that the layer thickness $d_{00.6}$ = 2.843 Å (calcite) practically coincides with the $d_{002}$ = 2.812 Å (zabuyelite), the related misfit being limited to 1.1%. From the crystal growth point of view, an important consequence arises. The epitaxially adsorbed $d_{002}$ zabuyelite layers can compete with the fresh $d_{006}$ calcite layers spreading on the pre-existing calcite face; due to the same thickness, calcite and zabuyelite layers encompass and overwhelm each other. As a final result, in perfect analogy with the adsorption/absorption sequence occurring in the case $\{111\}_{NaCl/formamide}$, zabuyelite layers are buried in the {00.1} calcite growth sectors. This has been experimentally proved by cathode-luminescence measurements (Fig. 14) and by XRPD diagrams. Hence, a new anomalous mixed crystal calcite/zabuyelite is generated, since only the {00.1} growth sectors is affected by the *ab*sorption of the epitaxially *ad*sorbed phase. As a matter of fact, when a deeper observation about the lithium effect is performed, a more complex behavior of the calcite crystals is evidenced. If one puts a calcite {10.4} rhombohedron as a seed in a lithium bearing growth solution, supersaturated with respect to calcite, then the {00.1} pinacoid begins to form and new growth layers propagate on both the pre-existing {10.4} faces and on new {01.8} faces, which took the place of the rhombohe-

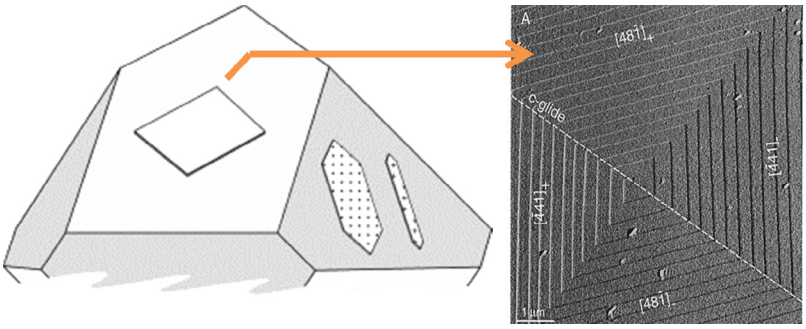


Fig. 12. (Left) The theoretical 2D growth islands on the {10.4} and {01.2} forms of calcite. (right) A growth spiral on the {10.4} form [28]: the directions of the growth steps, symmetry related by the glide **c** plane, reproduces those of the borders limiting the 2D islands drawn on the left side.

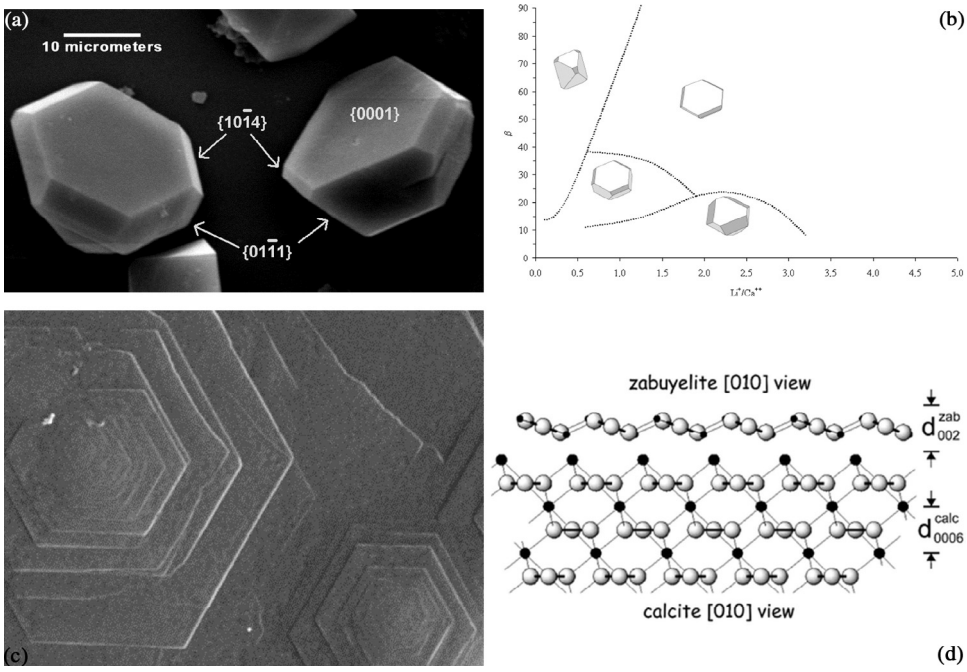


Fig. 13. Calcite crystals nucleated and grown from aqueous solution in the presence of varying concentrations of lithium: (a) the {00.1} pinacoid dominates on both cleavage and acute rhombohedra; (b) the "morphodrome" showing the habit change ({10.4} → {10.4} + {00.1}→{00.1}) with increasing lithium concentration and solution supersaturation (β); (c) SEM picture showing that the {00.1} form grows layer by layer and then assumes F character in the presence of lithium; (d) schematic drawing of the 2D epitaxy between the $d_{002}$ layers of lithium carbonate (zabuyelite) and the {00.1} substrate of the growing calcite; the quasi-equivalence of the thickness $d_{00.6}$ (calcite) and $d_{002}$ (zabuyelite) is highlighted as well. Adapted from Pastero et al. [24a]. Courtesy by ACS.

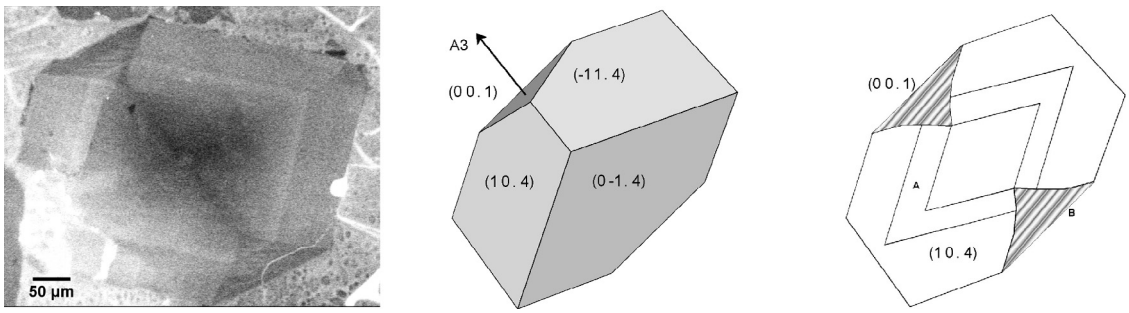


Fig. 14. (Left) Cathode-luminescence (CL) panchromatic image of the whole gel-grown calcite crystal, (center) corresponding crystal orientation, and (right) sector zoning (10.4) sector; funnel-shaped (00.1) sector.

dron edges (Fig. 15a). If the crystals continue growing, their morphology will be completely changed and the shape of the original seeds will disappear (Fig. 15b). It has been proven [24b] that the growth layers running on and covering both {10.4} and {01.8} faces can do it because the following 2D epitaxies can set up: $\{10.4\}_{calcite}$ /$\{001\}_{zabuyelite}$; $\{01.8\}_{calcite}$ /$\{001\}_{zabuyelite}$; $\{01.8\}_{calcite}$ /$\{100\}_{zabuyelite}$.

Summing up, this habit change is a spectacular case study, illustrating how much the morphology of a simple crystal can vary owing to the action of a simple ion added to the growth medium and, accordingly, how many mechanisms can be promoted. Lithium, as a monoclinic $Li_2CO_3$ crystal, can be epitaxially adsorbed on the {10.4} and {01.8} faces, modifying the character (from S to F) of the {01.8} flat rhombohedron; moreover, the epi-adsorption modifies as well the character (from K to F) of the {00.1} pinacoid and, at the same time the epi-adsorption is followed by the absorption of ordered crystalline $Li_2CO_3$ layers within the growth {00.1} sectors.

One of the most instructive cases, representing the complexity of the calcite growth forms, is that concern-

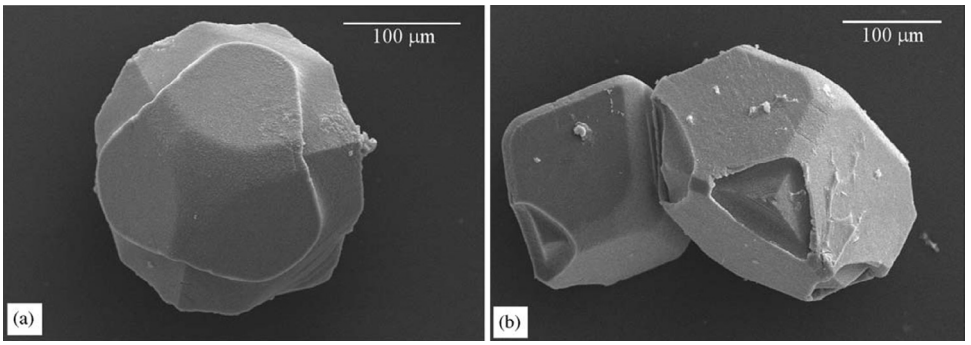


Fig. 15. (a) When a calcite crystal, initially showing the only {10.4} rhombohedron is put in a lithium bearing growth solution, new layers generate the {00.1} form and continue spreading on the adjacent pre-existing surfaces. Then, the {10.4} surfaces remain unaffected, while the {01.8} form takes the place of the rhombohedron edges. (b) Successively, the layers started from the {00.1} form encompass the crystal until the original morphology wholly disappears.

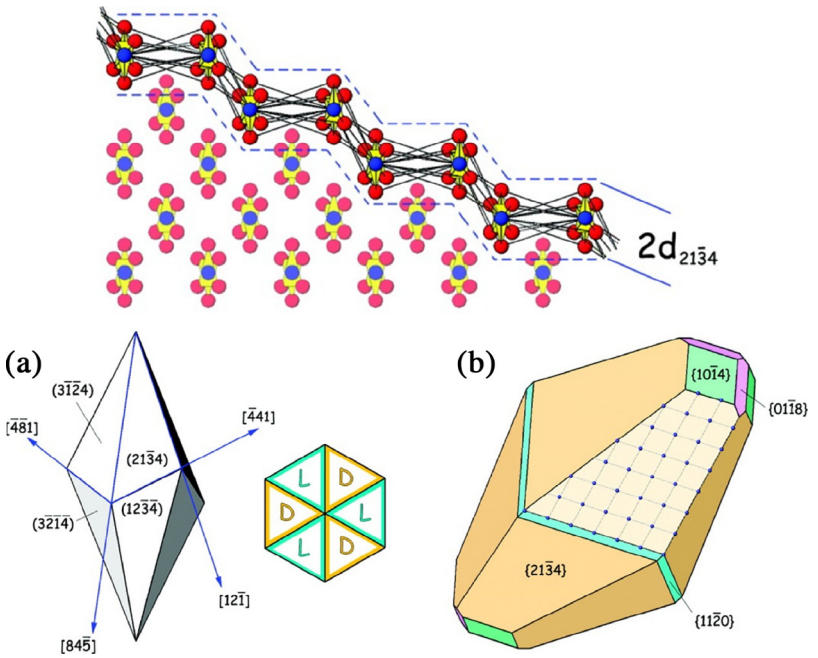


Fig. 16. (Top) The stepped profile of the {21.4} scalenohedron of calcite viewed along the < $\bar{4}$41 > zone axis. (bottom): (a) The scalenohedron with the directions of the edges between the equivalent faces. The up–down view along the [001] direction schematically represents the faces (D, L) related by the symmetry planes according to Hazen et al.'s labeling [29]. (b) All the forms belonging to the < $\bar{4}$41 > zone axis are represented, with the prevailing scalenohedron, for the sake of clarity. On the (21.4) face, the repeat 2D meshes of Ca ions lying in the outermost $d_{21.4}$ layer are also represented. Adapted from Aquilano et al. [24k]. Courtesy by ACS. (For interpretation of the references to colour in this figure legend, the reader is referred to the web version of this article.)

ing the {21.4} scalenohedron, which, surprisingly, is the second most frequently occurring form of natural calcites, as we mentioned above.

In Fig. 16 (top) the wavy stepped character of this form is illustrated along the right (D) and left (L) faces, mutually related by the symmetry planes (a-bottom). In Fig. 16 (b-bottom) a peculiar case of adsorption is drawn: herein, we will discuss this case in detail [24].

Hazen et al. [29] experimentally found that L-Aspartic molecules (L-Asp), versus D-Asp, adsorb preferentially on the L-faces of the scalenohedron while the inverse was found on the D-faces of the same form. Here, we would like to outline that the interpretation proposed by Hazen's group on the enantioselective adsorption is grounded on the interaction of a single molecule of the adsorbate with the crystalline substrate and the struc-

Table 1
Coincidence lattice and angular misfit between the (21.4) D-face of calcite and the (010) face of aspartic acid.

| Vector (Å) of the 2D coincidence cell on the (21.4) D-face of calcite | Vector (Å) of the 2D coincidence cell on the (010) face of aspartic acid | Misfit (%) |
|---|---|---|
| $3 \times 1/3\ [\bar{4}41] = 38.549$ | $5 \times [100] = 38.085$ | +1.22 |
| $4 \times 1/3[12\ \bar{1}] = 25.499$ | $5 \times [001] = 25.71$ | − 0.83 |
| $\varepsilon$ = angle $[\bar{4}41]\wedge[12\ \bar{1}] = 101.08°$ | $\gamma$ = angle $[100]\ \wedge\ [001] = 99.84°$ | Angular misfit +1.24° |
| 2D coincidence cell area = 964.64 Å$^2$ | 2D coincidence cell area = 964.76 Å$^2$ | 0.0012 |

ture of the substrate is not viewed as a set of well-ordered bond chains, which is physically sensible, but as a distribution of different atomic species at different levels with respect to the average crystallographic plane.

However, our way of thinking starts from the experience we gained in experimental and theoretical investigations on the adsorption/absorption phenomena occurring in calcium and barium carbonates growing from aqueous solutions in the presence of specific additives. Accordingly, we were induced to extend the model of 2D epitaxial adsorption to the interpretation of the enantioselectivity of the couple {21.4} calcite/aspartic acid.

Let us recollect the cell parameters (in Å) of the monoclinic and polar L-aspartic acid: $a_0 = 7.61$, $b_0 = 6.982$, $c_0 = 5.142$, $\beta = 99.84°$, and consider the $d_{020}$ slice, which is allowed by the systematic extinction rules. Owing to the $P2_1$ space group, this slice does show polarity along the [010] axis, due to the lack of the mirror symmetry (i.e., the 010 plane). Let us superimpose now the $d_{020}$ Asp slice onto the (21.4) D-face of calcite and turn it around its [010] axis until the $[100]_{Asp}$ and $[001]_{Asp}$ vectors coincide with the calcite scalenohedron edges $[\bar{4}41]$ and $[12\ \bar{1}]$, respectively. The excellent fit of the coincidence lattice occurring at the resulting calcite/Asp interface is illustrated in Table 1. Then, one is induced to hypothesize the occurrence of a 2D epitaxy between a $d_{020}$ slice of Asp and the (21.4) face of the calcite scalenohedron.

Further, the existence of Asp-epitaxial monolayers of thickness $d_{020} = 3.491$ Å implies a well-defined orientation of the Asp-molecules with respect to the scalenohedron substrate. In other words, the adsorbed monolayer must behave as a polar one; i.e., the (010) face of the monolayer is the complementary one of its opposite $(0\ \bar{1}0)$. Moreover, the (010) face of the crystalline L-Asp is the mirror image of the $(0\ \bar{1}0)$ face of D-Asp. This means that *the enantio-selectivity does not depend on the surface structure of the (21.4) and ($\bar{2}$3.4) faces of the scalenohedron* (which are symmetry equivalent), *but on the coupling between the substrate and the properly oriented epitaxial layer of molecules of suitable chirality*. This is a fundamental finding, because the 2D epitaxy of adsorbed polar layers does explain why the presence of a prevailing enantiomer (L or D) in the growth solution can differently affect the growth rate of L and D faces of the scalenohedron that, in the absence of this kind of adsorption, would grow at the same rate.

Table 2
Surface (relaxed and unrelaxed) energies ($\gamma_{hk.l}$, in erg cm$^{-2}$) in the $[\bar{4}41]$ zone of calcite.

| form and character | {10.4}-F | {11.0}-F | {01.8}-S | {21.4}-S |
|---|---|---|---|---|
| $\gamma_{unrelaxed}$ ($\gamma_u$) | 707 | 1812 | 1253 | 1451 |
| $\gamma_{relaxed}$ ($\gamma_r$) | 536 | 1232 | 702 | 783 |
| $\Delta\gamma\ (\%) = (\gamma_r - \gamma_u)/\gamma_u$ | 24.18 | 32.01 | 43.97 | 46.04 |

This reasoning is also fundamental to understand why a stepped form as the {21.4} could be so important in the growth morphology. In fact, from Table 2, one could argue that {21.4} cannot enter the equilibrium shape of calcite, even if the surface relaxation strongly reduces its surface energy value; nevertheless, if the above mentioned adsorption is considered, another severe $\gamma$ reduction will affect the {21.4} form and then it could enter the equilibrium shape. It follows that this 2D epitaxy would affect both the shape of calcite at the nucleation stage and the shape of the growing crystals, due to its hindering action on the {21.4} terraces, with respect to the incoming flow of calcium and carbonate ions of the supersaturated mother phase.

## 4. Gypsum ($CaSO_4 \cdot 2H_2O$, space group C2/c)

Gypsum (calcium sulfate dihydrate, $CaSO_4 \cdot 2H_2O$) is the most abundant natural sulfate. It is widely present in the earth crust and plays important roles in various geological (for instance crustal deformation dynamics) and environmental (for instance the global distribution of $Ca^{2+}$ and $SO_4^{2-}$) processes. Gypsum is also heavily used in industry, as a construction material (plaster, mortar, blocks, additive to Portland cement, etc.), a component of fertilizers and soil conditioners for high sodium soils, and even in the cosmetic (foot creams, shampoos and other hair products) and food (tofu, dough conditioner, brewery, etc.) industry.

Calcium sulfate scaling is a major issue in applications such as desalination, geothermal energy produc-

tion, and petroleum engineering. Crystalline deposits formed during these processes are detrimental to the efficiency of the processes, which has encouraged much work to characterize the gypsum precipitation behavior and the development of scale inhibitors that modify the crystal morphology or prevent the adhesion of crystals to surfaces.

The aim of most studies on gypsum crystallization up to now has been to understand the influence of additives on the nucleation and growth kinetics and the morphology of crystals. A large number of papers can be found on this topic (see for example Fan and Teng (2011) for a review [30]). In this section the study of gypsum without any additives is summarized, with emphasis on the growth mechanisms and the morphology, that are the key elements in terms of applied crystallization.

Recently, gypsum crystallization has gained further interest owing to the study of naturally appearing giant crystals in Naica (Mexico), which have been proven to grow very close to equilibrium. This make these crystals, having some unexpected morphologies, an ideal workbench for close to equilibrium crystal growth studies, a field in which experiments other than these natural realizations are very difficult of impossible. Some advances in the understanding of gypsum crystallization triggered by studies on these natural crystals will be commented. The giant gypsum crystals at Naica are a nice example of the two-way benefits of studying mineral crystal growth. On one side, natural crystals often grow under conditions that are difficult or impossible to reproduce in the laboratory, thus giving very useful information on crystal growth processes in these conditions. On the other side, the understanding of mineral crystal growth allows us to derive physical and chemical information from the properties of the crystals found in geological setting, being excellent clues to understand geological processes. More information on this second point of view can be found in a review by García-Ruiz and Otálora [31].

### 4.1. Crystallography

The structure of gypsum (monoclinic system) consists of layers of $SO_4^{2-}$ tetrahedra, which are bound together by $Ca^{2+}$ cations. Water molecules are arranged between these layers (Fig. 17).

The anisotropy of the structure is evident. Gypsum has a perfect 010 cleavage, owing to the structural layers of water molecules linking the building slabs of $SO_4^{2-}$ tetrahedra with thickness $d_{020} = 7.575$ Å. The cleavage planes run through the weak H-bonds formed by the water molecules. The presence of water molecules in these layers

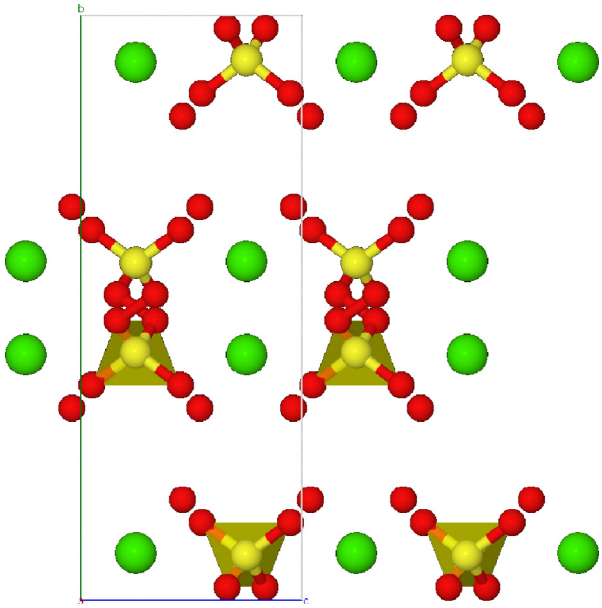


Fig. 17. Structure of gypsum as seen along the a direction. Some of the $SO_4^{2-}$ tetrahedra are shown at the bottom. Hydrogen from the water molecules are not shown to visually highlight the H-bonding layers perpendicular to the b direction. A perpendicular view (along b) is shown in Fig. 18. (For interpretation of the references to colour in this figure legend, the reader is referred to the web version of this article.)

also controls crystal growth and morphology, because crystal faces other than {010} present alternating regions of water and $SO_4$/Ca with very different bonding energy.

As with any other crystal, the assignment of the unit cell for gypsum is not univocal. But in the case of gypsum several such selections are reasonable and have been made by different authors. This is a potential source of confusion and mistakes, since the indexing of crystallographic surfaces and directions change with the reference frame chosen. Three main conventions have been used for gypsum (length of parameters in Å) [32]:

- $a_1 = 5.63$, $b_1 = 15.15$, $c_1 = 6.23$, $\beta_1 = 113.83°$, used by de Jong and Bouman (1939) [33] (C2/c), Cole and Lancucki (1974) [34] (A2/a) or Heijnen and Hartman (1991) [35] (A2/a),
- $a_2 = 6.28$, $b_2 = 15.15$, $c_2 = 6.51$, $\beta_2 = 127.40°$, used by Ramdohr et al. (1978) [36] (A2/a) or Boeyens and Icharam (2002) [37] (C2/c)
- $a_3 = 5.67$, $b_3 = 15.15$, $c_3 = 6.51$, $\beta_3 = 118.38°$, used by Bragg et al. (1965) [38] (I2/a), Pake (1948) [39] (I/2a) or Pedersen and Semmingsen (1982) [40] (I2/a)

The three reference systems are illustrated in Fig. 18, the indexing of the common faces of the gypsum mor-

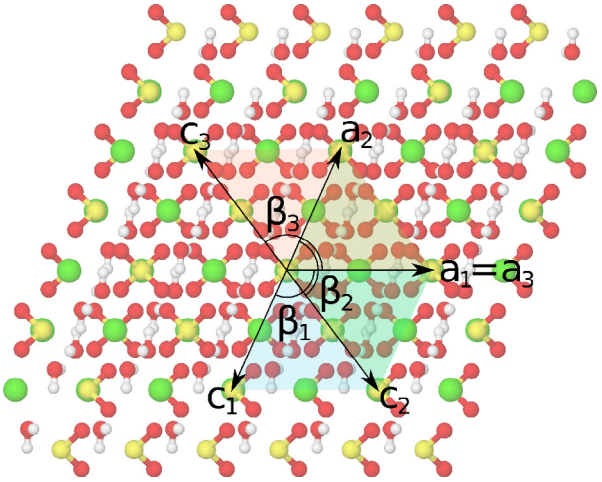


Fig. 18. Reference frames often used to index gypsum crystals superimposed on the atomic structure projected along the b direction (this direction is perpendicular to the paper in all cases (from paper to the reader in references 1 and 2, and from the reader to paper in reference 3). The crystallographic a and c directions are shown for the first three systems discussed in the text along with the respective unit cells shown as transparent blue, green and orange polygons. (For interpretation of the references to colour in this figure legend, the reader is referred to the web version of this article.)

phology using these reference systems is illustrated in Fig. 19. They are related as:

$$a_2 = -c_1, b_2 = b_1, c_2 = a_1 + c_1$$

$$a_3 = a_1, b_3 = -b_1, c_3 = -(a_1 + c_1)$$

In this paper we will use the reference frame by de Jong and Bouman, since it is the most suitable to work with the growth morphology of gypsum; it's not unintentional that this frame, along with the analogues by Cole–Lancucki and Heijnen–Hartman have been called as "morphological cell."

Other indexing frames can be found in the literature such as

- $a_4 = 10.47$, $b_4 = 15.15$, $c_4 = 6.28$, $\beta_1 = 98.97°$,
- $a_5 = 10.47$, $b_5 = 15.15$, $c_4 = 6.51$, $\beta_{12} = 151.55°$,

but they are of relatively less importance and, consequently, not shown in Fig. 18.

The hkl indices of crystallographic features in previous literature must be converted from the reference frame of the original paper to the one selected. To do it, the equation

$$\vec{h}_j = M\vec{h}_i$$

is used, where $\vec{h}_i$ and $\vec{h}_j$ are the indices (column vector) in the old and new reference systems respectively and $M$ in one of the following transformation matrices:

| | From 1 | From 2 | From 3 |
|---|---|---|---|
| To 1 | $M = \begin{pmatrix} 1 & 0 & 0 \\ 0 & 1 & 0 \\ 0 & 0 & 1 \end{pmatrix}$ | $M = \begin{pmatrix} 0 & 0 & 1 \\ 0 & 1 & 0 \\ 1 & 0 & 1 \end{pmatrix}$ | $M = \begin{pmatrix} 1 & 0 & -1 \\ 0 & -1 & 0 \\ 0 & 0 & -1 \end{pmatrix}$ |
| To 2 | $M = \begin{pmatrix} -1 & 0 & 1 \\ 0 & 1 & 0 \\ 1 & 0 & 0 \end{pmatrix}$ | $M = \begin{pmatrix} 1 & 0 & 0 \\ 0 & 1 & 0 \\ 0 & 0 & 1 \end{pmatrix}$ | $M = \begin{pmatrix} -2 & 0 & 1 \\ 0 & -1 & 0 \\ -1 & 0 & 0 \end{pmatrix}$ |
| To 3 | $M = \begin{pmatrix} 1 & 0 & -1 \\ 0 & -1 & 0 \\ 0 & 0 & -1 \end{pmatrix}$ | $M = \begin{pmatrix} 0 & 0 & -1 \\ 0 & -1 & 0 \\ 1 & 0 & -2 \end{pmatrix}$ | $M = \begin{pmatrix} 1 & 0 & 0 \\ 0 & 1 & 0 \\ 0 & 0 & 1 \end{pmatrix}$ |

The corresponding transformation of the form indices is shown in Fig. 19.

### 4.2. Morphology

Gypsum is also an excellent model for crystal morphology. Traditional methods to compute the equilibrium shape of a crystal are based on the minimization of the surface energy of the ensemble of atoms limiting the anisotropic solid [10,11]. Several methods have been used to this end, among which the Periodic Bond Chains formalism [22], is the one used most often. The structural morphology of gypsum was first investigated using this method by Simon and Bienfait [41], who calculated the electrostatic attachment energies for the F faces. The stability of the monolayered steps building the 2D nuclei on all the flat (F) forms was also determined by these authors. They calculated both the theoretical equilibrium and growth shapes to be platy {010}-dominated crystals bounded by faces {010}, {120}, {011} and {-111} (Fig. 20a) but, as they themselves recognized in this first article, "the agreement with the observed habit is not particularly good, and this is shown to be the consequence of the adsorption of the solvent on faces and edges of the crystal." The limitations of the methods to compute crystal morphology show up in this lack of agreement:

- The crystal is assumed to be in vacuum so they usually fail when solvent interactions are important like in hydrated crystals like gypsum.
- Only F forms are considered for the analysis, while S and K forms can enter the growth morphology of crystals by generating new periodic bond chains through temporary solvent and/or impurity adsorption at the surface.

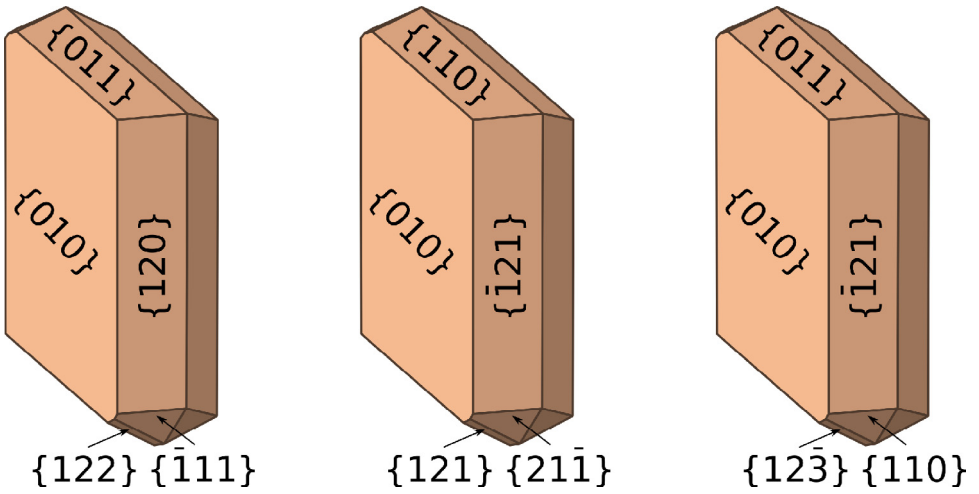


Fig. 19. Typical morphology of a gypsum crystal showing the forms indexed using reference systems 1 (left), 2 (center) and 3 (right).

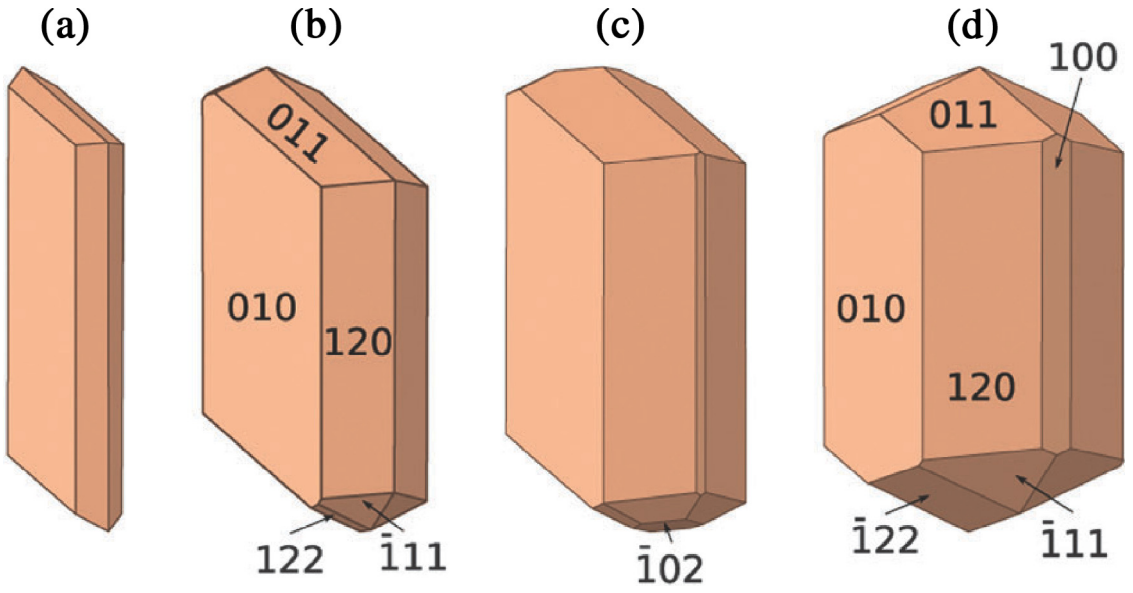


Fig. 20. Selection of equilibrium morphologies for gypsum from literature. All indices refer to forms, not individual faces. (a) PBC morphology (Simon and Bienfait [41,42]), (b) refined PBC morphology (Van der Voort and Hartman [43]), (c) minimized surface energy morphology without surface relaxation and (d) with surface relaxation (both from Massaro et al. [44a]). Reprinted with permission from Otálora and García-Ruiz [45]. Copyright © 2010, RCS.

- Atoms and molecules at the surface of the crystal are assumed to be rigidly fixed at the crystallographic positions defined by the structure; i.e. no surface reconstructions that may change the surface energy are usually taken into account.
- No knowledge on the crystal growth unit (the individual units incorporating into the surface from the solution) is incorporated so layers having a thickness $d_{hkl}/2$, $d_{hkl}/3$, $d_{hkl}/4\ldots$ must be considered as candidate surface layers (provided they are consistent with the crystal structure and symmetry).

The first problem was identified by Simon [42] and further investigated by Van der Voort and Hartman [43] who realized that two kinds of water molecules can be present on the crystal faces: one that belongs to the crystal structure and is not removed when the face advances, and the other one that does not belong to the crystal structure and must be desorbed before the face can continue growing. They proposed that the first situation happens in the case of the {011} form while the second one is the case of the {1111} form. Consequently, the growth rate of {111} is reduced with respect to that of {011} due

to this extra energy required for surface dehydration, ending up as a face much more developed, in good agreement with the experimentally observed morphology of gypsum.

Weijnen et al. [46], investigating the adsorption of additives at the gypsum crystal surfaces using a different method (broken bond model and critical Ising temperatures), were the first to consider how slices $d_{hkl}/2$ thick can exist on both {011} and {111} forms, as theoretically suggested by Hartman and Heijnen [47]. They were unable to conclusively determine weather full or half slice growth happens in each of the faces. This important point was later faced by Heijnen and Hartman [48]; they found that both the {011} and {111} forms can grow by half slices and that the difference in attachment energy between full and half slices is smaller for {011} than for {111}. The (011) face can therefore start growing by half slices at lower supersaturations than (111), which can be the reason for the faster growth of (011) and the larger relative development of (111). Furthermore, they also found that {122} is another F form and obtained theoretical habits that are tabular {010} and contain the forms {120}, {011}, and {111}, in order of decreasing importance. These habits were reasonably close to most of the known gypsum single crystals.

The discovery of the giant gypsum crystals in Naica (Mexico) in 2000 raised new questions on the morphology of gypsum. A genetic model was soon proposed [49] that identified them as a result of crystal growth at very low supersaturation over a very long time period. The morphology of the crystals can therefore be assumed to be very close to the equilibrium morphology, but it happens to be different from the equilibrium shape known at the time. Two types of crystals, already described in other nearby cave by Foshag [50], are present in the Cave of Crystals in Naica the "blocky crystals" and the "beams." Both habits show prisms bounded by {010} and {1k0} faces and capped by {-111} faces [49]. The more developed faces are the {1k0} family instead of {010}, several faces in this family alternating (at least) $2 \le k \le 6$ with {010} segments and composing an overall surface is the direction of {140} instead of {120}. These two features don't agree with the equilibrium shape known at the time.

Aquilano and coworkers reexamined the morphology of gypsum finding that more accurate models for the crystal surface could explain all these features [44a–c]. These models predict that the traditionally dominant {010} pinacoid is overtaken by the {120} prism and new stepped forms, {100} and $\{12\bar{2}\}$ along with the kinked {102} form, enter into the equilibrium shape. The equilibrium shape of gypsum shows not only flat faces but also the {140} and {180} stepped forms and probably also the stepped {130} and {170} forms. Using energy minimization methods, these authors showed that the reorientation of water molecules modifies the coordination of water molecules and the number of unsaturated bonds exposed. In the case of the {120}, {130}, {140} forms, the surface is more solvated and closer to a deeper energy minimum, which can explain their presence in the striated surfaces observed in Naica crystals. The resulting equilibrium morphology is dominated by four F forms, {010}, {120}, {011} and {111}, and smoothed by four S forms, {100}, $\{12\bar{2}\}$, {140}, {180}, and by the K form {102}, which shows that the contribution of the surface relaxation is not negligible.

These increasingly accurate studies on the equilibrium morphology are much more relevant than it might seem. The specific surface energy of the different anisotropic surfaces is a key parameter in crystal growth, governing not only crystal habit but also nucleation and growth kinetics. The discrepancies in the surface energy of gypsum observed during the development of morphological studies could also be a reason for still open and important problems like the relative stability fields of anhydrite and gypsum, which show important discrepancies between thermodynamics theory and experiments, because specific surface energy is the main control of nucleation.

Even more characteristic than equilibrium morphology of gypsum is the twinning of these crystals, which is a distinctive characteristic of gypsum [51,52]. Five twin laws of gypsum (100, 001, 10-1, 201 and 101) have been reported [53–56], as shown in Fig. 21. It is interesting to note that none of the respective composition planes have F character (the first three are S surfaces while the last two are K forms). The twin energies varies widely for the five twins with $\gamma_{PT}$ values of 13.6, 145, 255, 826, and 848 erg $cm^{-2}$ for the 100, 001, -101, 201 an 101 laws respectively. Among these twin laws, 100 seems to be the more frequent one, both because the twin energy is smaller and because (100), in spite of being an S face, belongs to the equilibrium shape of the crystal.

In addition to their widespread presence in laboratory and natural gypsum crystals and their importance for practical problems related to the production of gypsum crystals or anti-scale methods, gypsum twins could also play an important role in the growth of crystals at low supersaturation. The reentrant angle of twinned gypsum crystals may work as a potential source of steps that enhances growth and modifies the resultant crystal morphology. Given the scarcity of screw dislocations sources commented before, this mechanism could be important in low supersaturation growth of gypsum crystals. This

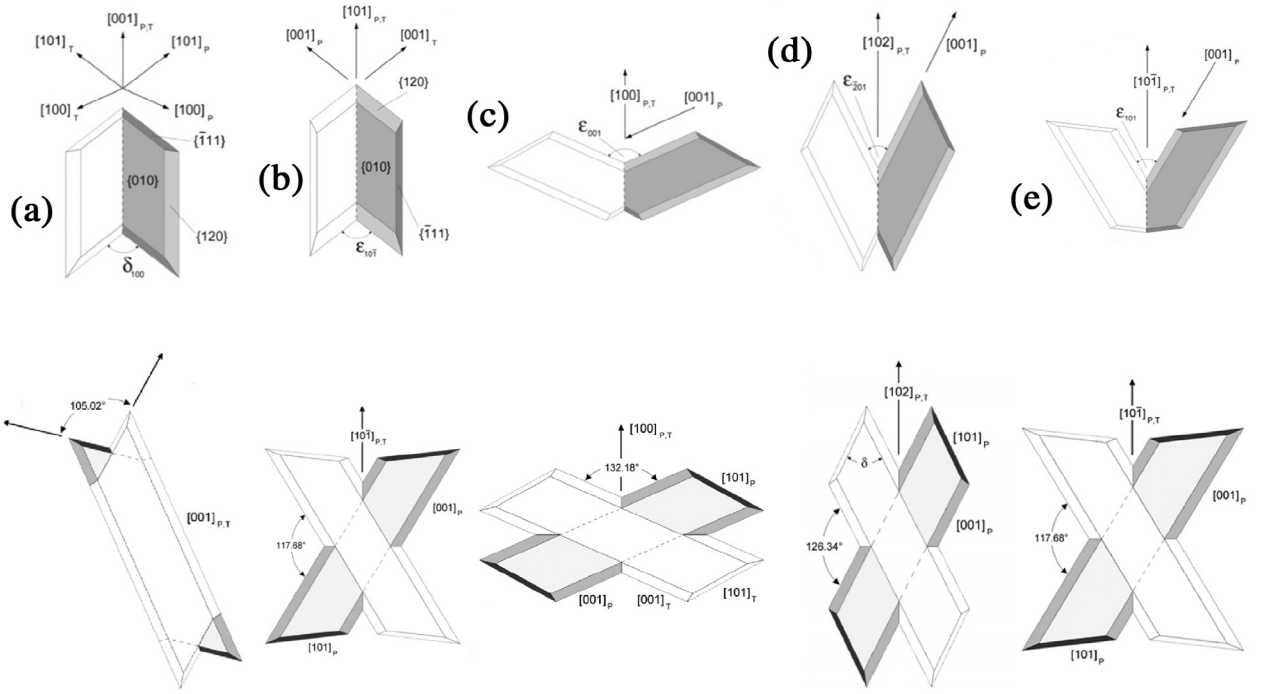


Fig. 21. Top: contact twins of gypsum viewed along the [010] direction. Twin laws: 100 (a), $\bar{1}01$ (b), 001 (c), 20 (d), and 10 $\bar{1}$(e). For each law, the contact twins have been drawn assuming that the growth rate of both {120} and { $\bar{1}01$} prisms is lower than that of the {010} pinacoid. Dashed lines represent contact planes. P and T stand for parent and twinned individuals, respectively. It is worth nothing that $\delta_{100} = \varepsilon_{\bar{1}01} = 105.02°$. Bottom: the corresponding penetration twins of the top row (obviously, from top to bottom the twin axes, for each twin law, have been rigorously maintained). Adapted from Rubbo et al. [54,55]. Courtesy by ACS.

mechanism has been proposed [45] as the reason for the formation of the long beams (up to 11 meters) in the Cave of Crystals at Naica.

### 4.3. Growth mechanisms

Virtually all studies on gypsum growth mechanisms have been performed on the {010} form, while the growth mechanisms of other faces remain almost completely unknown. Most of these studies have been performed on cleavage surfaces by using AFM alone [52,57–62], AFM in combination with LCDCIM [63] or Phase Shift Michelson Interferometry [64].

The presence of dislocation outcrops on the {010} form has been reported in dissolution experiments as equal spaced pits linearly arranged along the 010 cleavage planes of natural crystals, but they are not screw dislocations. Raju (1980) concluded that they correspond to low-angle grain boundaries consisting of equispaced edge dislocations [65]. The presence of these edge dislocations was also confirmed by X-ray topography studies [66]. Although some studies on bulk crystal growth kinetics in the low supersaturation range and SEM images of gypsum suggest that growth kinetics are consistent with spiral growth as the main growth mechanism [67,68], screw dislocations are infrequently observed on the {010} form of gypsum crystals during in situ experiments. In fact, screw dislocation hillocks have been only reported by Driessche et al. [63] as a very infrequent feature. So 2D nucleation seems to be the main source of growth steps at any supersaturation value.

The first study of the {010} surfaces of gypsum crystals using AFM (Shindo et al. [57] concentrated on the atomic level structure of the crystal surface, showing some degree of rearrangement of the molecules at the crystal surface and the rigid adsorption of the water molecules onto the surface. Bosbach and Rammensee [58] showed that the growth and dissolution on the (010) surface in aqueous solution is a layer-by-layer process and that the distinctive step directions (parallel to [001], [100], and [101]) move with strongly anisotropic velocity. After a two-dimensional nucleus form, growth occurs via advancing steps. For monolayered steps, the velocity of [101] steps is higher, relative to [001] steps, which is a result of higher step energy for [101] steps. The step velocity of [101] steps is further increased in the presence of NaCl, whereas [001] steps advance with identical velocities in the presence of NaCl. The step velocity was measured

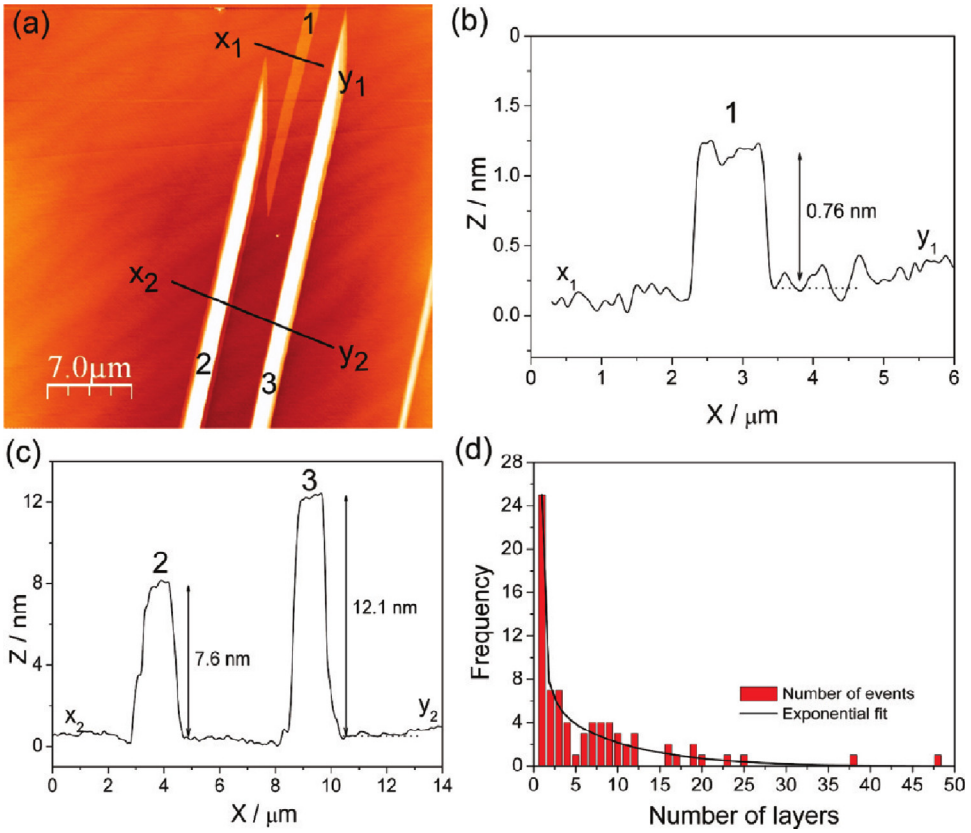


Fig. 22. In situ AFM image (a) and profiles showing monolayer (b) and multilayer (c) islands growing on the {010} gypsum face in contact with a supersaturated $CaSO_4$ solution. (d) Histogram representation of the frequency of multilayer 2D islands observed as a function of the number of layers they contain. (from reference Van Driessche et al. [63]). Reprinted with permission from Van Driessche et al. [63]. Copyright © 2010, ACS. (For interpretation of the references to colour in this figure legend, the reader is referred to the web version of this article.)

to be up to 30.0 nm $s^{-1}$ for isolated [100] monolayer steps, up to 9.5 nm $s^{-1}$ for [010] steps and 2.5 nm $s^{-1}$ for [001] steps. Individual kink sites were observed and its formation energy along [001] steps determined (4.1 ± 0.7 KJ mol-1) in saturated aqueous solution. Van Driessche et al. [63] also observed steps roughly oriented along [102].

Macrosteps have been also reported in addition to monolayer steps (Fig. 22). The height of monolayers is approximately 7–8 Å, corresponding to about one-half of the b-axis length (Bosbach and Rammensee [58], Bosbach and Hochella Jr. [60], Bosbach et al. [52], Van Driessche et al. [63]). Large, isolated 2D islands bounded by macrosteps are shown by Van Driessche et al. [63]. The frequency of these high islands decrease exponentially with height, but some of them made of more than 20 monolayers have been observed. The mechanism of formation of these multilayer islands is yet not known, and can be an important contribution to the growth kinetics at low supersaturation.

Studies on the effect of additives on the atomic-level topography of the {010} face of gypsum show an strong impact of phosphonate [58]. Adsorbed HEDP and ENTMP molecules were attached to step edges, resulting in a change in step morphology. Inhibitor concentration and the reactivity of step edges seem to be the main factor controlling the step morphology in these situations. Ex-situ images of gypsum crystals exposed to tartaric acid reveal that an amorphous coating has been precipitated at high tartrate concentrations, whereas low tartrate concentrations result in jagged or curved steps. [101] steps show the most significant change in step morphology: at low inhibitor concentrations linear steps become jagged, whereas high inhibitor concentrations lead to smoothly curved step edges. On the (010) surface, [101] steps are more reactive compared to [001] steps. In-situ experiments in the presence of citrate clearly show reduced growth rates. In-situ SFM experiments confirm the increased inhibition effect of phosphonic acid derivatives compared to carboxylates.

## Acknowledgments

D.A. and L.P. are grateful to Marco Rubbo and Marco Bruno (DST-Torino) for their fruitful discussion and co-operation. J.M.G-R. and F.O. acknowledge funding from the European Union's Seventh Framework Programme (FP7/2007-2013)/ERC grant agreement n° 340863, and from the Ministerio de Economía y Competitividad, proyecto CGL2013-43371-P.

## References

[1] M. Bienfait, R. Boistelle, R. Kern, Formes de croissance des halogénures alcalins dans un solvant polaire, in: CNRS (Ed.), Coll. Intern, n° 152, Adsorption et Croissance Cristalline, Paris, 1965, pp. 577–594.

[2] M. Romé de l'Isle, Cristallographie ou description des formes propres à tous les corps du regne minéral, dans l'état de combinaison saline, pierreuse ou métalliques, 4 vol, second ed., Paris, 1783.

[3] F. Gille, K. Spangeberg, Beiträge zur Trachtbeeinflussung des NaCl durch Harnstoff als Lösungsgenossen, Z. Kristallographie 65 (1–6) (1927) 204–250.

[4] P. Hartman, Le coté cristallographique de l'adsorption vu par le changement de faciès, in: CNRS (Ed.), Coll. Intern, n° 152, Adsorption et Croissance Cristalline, Paris, 1965, pp. 477–513.

[5] L. Royer, Des matières étrangères qui, ajoutées à l'eau mère d'une solution, sont susceptibles de modifier le faciès des cristaux du corps dissous, Comptes rendus Acad. Sci., Paris, 1934, p. 198. 185–187; ibid. 585; ibid. 949; ibid. 1868.

[6] R. Boistelle, B. Simon, Epitaxies de $CdCl_2{\cdot}2NaCl\cdot 3H_2O$ sur les faces (100), (110) et (111) des cristaux de chlorure de sodium, J. Cryst. Growth 26 (1974) 140–146.

[7] L. Pastero, D. Aquilano, M. Moret, Selective adsorption/absorption of formamide in NaCl crystals growing from solution, Cryst. Growth Des. 12 (2012) 2306–2314.

[8] (a) N. Radenoviĉ, D. Kaminski, W. Van Enckevort, S. Graswinkel, I. Shah, M. In't Veld, et al., Stability of the polar {111}NaCl crystal faces, J. Chem. Phys. 124 (2006) 164706; (b) N. Radenović, W. Van Enckevort, E. Vlieg, Formamide adsorption and habit changes of alkali halide crystals grown from solution, J. Cryst. Growth 263 (2004) 544–551; (c) E.R. Townsend, W.J.P. van Enckevort, J.A.M. Meijer, E. Vlieg, Polymer versus monomer action on the growth and habit modification of sodium chloride crystals, Cryst. Growth Des. 15 (2015) 5375–5381.

[9] D. Aquilano, L. Pastero, M. Bruno, M. Rubbo, {100} and {111} forms of the NaCl crystals coexisting in growth from pure aqueous solution, J. Cryst. Growth 311 (2009) 399–405.

[10] (a) P. Curie, Crystals and crystallization, Bull. Soc. Min. Fr. 91 (7) (1885) 418; (b) W. Gibbs, On the equilibrium of heterogeneous substances: abstract by the Author, Am. J. Sci. 3 ser. XVI (1878) 441–458.

[11] G. Wulff, Zur frage der Geschwindigkeit des Wachstums und der Auflösung der Krystalflachen, Z. Kristallogr. 34 (1901) 449–530.

[12] (a) I.N. Stranski, Zur Theorie der Kristallwachstums, Z. Phys. Chem. 138 (1928) 259–277; (b) F. Bertaut, Le terme éléctrostatique de l' énergie de surface, C. R. 246 (1958) 3447–3450; (c) P. Hartman, Sur la structure atomique de quelques faces des crystaux du type blende et wurtzite, Bull. Soc. Fr. Minér. Crist. 82 (1959) 158–163.

[13] W. Hebenstreit, M. Schmid, J. Redinger, R. Podloucky, P. Varga, Bulk terminated NaCl (111) on aluminum: a polar surface of a ionic crystal?, Phys. Rev. Lett. 85 (2000) 5376.

[14] R. Lacmann, Gleichgewichtsform und Oberflachenstruktur von NaCl Kristallen, in: CNRS (Ed.), Coll. Intern, 152, Adsorption et Croissance Cristalline, Paris, 1965, pp. 195–214.

[15] D. Knoppik, A. Lösch, Surface structure and degree of coarsening of {111} NaCl surfaces near the thermodynamic equilibrium between crystal and vapour, J. Cryst. Growth 34 (1976) 332–336.

[16] M. Bruno, D. Aquilano, L. Pastero, M. Prencipe, Structures and surface energies of {100} and octopolar {111} faces of Halite (NaCl): an ab initio quantum-mechanical and thermodynamical study, Cryst. Growth Des. 8 (2008) 2163–2170.

[17] R. Kern, The equilibrium form of crystals, in: I. Sunagawa (Ed.), Morphology of Crystals, Part A, Terra Sci. Publ. Co., Tokyo, 1987, pp. 77–203.

[18] W.D. Harkins, H.M. McLaughlin, The structure of films of water on salt solutions. I. Surface tension and adsorption for aqueous solutions of sodium chloride, J. Am. Chem. Soc. 47 (1925) 2083–2089.

[19] R. Bahadur, L.M. Russell, S. Alavi, Surface tensions in NaCl–water–air systems from MD simulations, J. Phys. Chem. B 111 (2007) 11989–11996.

[20] W. von Engelhardt, Untersuchungen über den Randwinkeln von Flüssigkeiten auf Kristalloberflächen, in: CNRS (Ed.), Coll. Int., 152, Adsorption et Croissance Cristalline, Paris, 1965, pp. 119–137.

[21] W.M.M. Heijnen, The morphology of gel grown calcite, Neues Jahrb. Miner. Mh. 8 (1985) 357–371.

[22] P. Hartman, Modern PBC Theory, Ch.4, in: I. Sunagawa (Ed.), Morphology of crystals, Terra Sci. Publ. Co, Tokyo, 1987, pp. 269–319.

[23] (a) S.C. Parker, E.T. Kelsey, P.M. Oliver, J.O. Titiloye, Computer modelling of inorganic solids and surfaces, Faraday Discuss. 97 (1993) 75–84; (b) N.H. de Leeuw, S.C. Parker, Atomistic simulation of the effect of molecular adsorption of water on the surface structure and energies of calcite surfaces, J. Chem. Soc. Faraday Trans. 93 (1997) 467–475; (c) J.O. Titiloye, N.H. de Leeuw, S.C. Parker, Atomistic simulation of the differences between calcite and dolomite surfaces, Geochim. Cosmochim. Acta 64 (1998) 2637–2641; (d) N.H. de Leeuw, S.C. Parker, Surface structure and morphology of calcium carbonate polymorphs calcite, aragonite, and vaterite: an atomistic approach, J. Phys. Chem. B 102 (1998) 2914–2922; (e) S. Hwang, M. Blanco, W.A. Goddard, Atomistic simulations of corrosion inhibitors adsorbed on calcite surfaces. I. Force field parameters for calcite, J. Phys. Chem. B 107 (2001) 10746–10752; (f) S.C. Parker, S. Kerisit, A. Marmier, S. Grigoleit, G.W. Watson, Modelling inorganic solids and their interfaces: a combined approach of atomistic and electronic structure simulation techniques, Faraday Discuss. 124 (2003) 155–170.

[24] (a) L. Pastero, E. Costa, M. Bruno, G. Sgualdino, D. Aquilano, Morphology of calcite ($CaCO_3$) growing from aqueous solutions in the presence of $Li^+$ ions. Surface behaviour of the {00.1} form, Cryst. Growth Des. 4 (2004) 485–490; (b) L. Pastero, D. Aquilano, E. Costa, M. Rubbo, 2D epitaxy of lithium carbonate inducing growth mechanism transitions on {00.1}-K and {01.8}-S

forms of calcite crystals, J. Cryst. Growth 275 (2005) e1625–e1630; (c) M. Bruno, M. Prencipe, Ab initio quantum-mechanical modeling of the (001), (01) and (110) surfaces of zabuyelite ($Li_2CO_3$), Surf. Sci. 601 (2007) 3012–3019; (d) L. Pastero, F.R. Massaro, D. Aquilano, Experimental and theoretical morphology of single and twinned crystals of $Li_2CO_3$ (zabuyelite), Cryst. Growth Des. 7 (2007) 2749–2755; (e) F.R. Massaro, L. Pastero, E. Costa, G. Sgualdino, D. Aquilano, Single and twinned $Li_2CO_3$ crystals (Zabuyelite) epitaxially grown on {00.1} and {10.4} forms of $CaCO_3$ (Calcite) crystals, Cryst. Growth Des. 8 (2008) 2041–2046; (f) L. Pastero, D. Aquilano, $CaCO_3$ (calcite)/ $Li_2CO_3$ (zabuyelite) anomalous mixed crystals. Sector zoning and growth mechanisms, Cryst. Growth Des. 8 (2008) 3451–3460; (g) M. Bruno, F.R. Massaro, M. Prencipe, Theoretical structure and surface energy of the reconstructed {01.2}form of calcite ($CaCO_3$) crystal, Surf. Sci. 602 (2008) 2774–2782; (h) F.R. Massaro, M. Bruno, D. Aquilano, Effect of the surface relaxation on the theoretical equilibrium shape of calcite. I. The [001] zone, Cryst. Growth Des. 10 (2010) 4096–4100; (i) M. Bruno, F.R. Massaro, M. Prencipe, D. Aquilano, Surface reconstructions and relaxation effects in a centre-symmetrical crystal: the {00.1}form of calcite ($CaCO_3$), CrystEngComm 12 (2010) 3626–3633; (j) M. Bruno, F.R. Massaro, M. Rubbo, M. Prencipe, D. Aquilano, The (10.4), (01.8), (01.2) and (00.1) twin laws of calcite ($CaCO_3$): equilibrium geometry of the twin boundary interfaces and twinning energy, Cryst. Growth Des. 10 (2010) 3102–3109; (k) D. Aquilano, M. Bruno, F.R. Massaro, M. Rubbo, On the theoretical equilibrium shape of calcite. 2. The [/41] zone and its role in biomineralization, Cryst. Growth Des. 11 (2011) 3985–3993; (l) D. Aquilano, R. Benages-Vilau, M. Bruno, M. Rubbo, F.R. Massaro, Positive and negative forms of calcite ($CaCO_3$) crystal. New open questions from the evaluation of their surface energies, CrystEngComm 15 (2013) 4465–4472; (m) M. Bruno, F.R. Massaro, L. Pastero, E. Costa, M. Rubbo, M. Prencipe, et al., New estimates of the free energy of calcite/water interfaces for evaluating the equilibrium shape and nucleation mechanisms, Cryst. Growth Des. 13 (2013) 1170–1179; (n) M. Bruno, The free energy density of a crystal: calcite ($CaCO_3$) as a case of study, CrystEngComm 17 (2015) 2204–2211.

[25] A.L. Rohl, K. Wright, J.D. Gale, Evidence from surface phonons for the $(2 \times 1)$ reconstruction of the (10.4) surface of calcite from computer simulation, Am. Miner. 88 (2003) 921–925.

[26] I. Sunagawa, Variation of crystal habit of calcite, Geol. Surv. Japan Rep. 155 (1953) 1–66.

[27] V. Goldschmidt, Atlas der Kristallformen (1913), Tafeln Band II, pp. 1–7.

[28] H.H. Teng, P.M. Dove, J.J. de Yoreo, Kinetics of calcite growth: surface processes and relationships to macroscopic rate laws, Geoch. Cosmoch. Acta 64 (2000) 2255–2266.

[29] (a) R.M. Hazen, T.R. Filley, G.A. Goodfriend, Selective adsorption of L- and D- amino-acids on calcite: implication for biochemical homochirality, Proc. Natl. Acad. Sci. U.S.A. 100 (2001) 5487–5490; (b) R.M. Hazen, J.A. Brandes, H.S.J. Yoder., Possible roles of mineralsin the prebiotic synthesis and selectioon of amino acids, Trans. Am. Geophys. Union (Abstract) 2002; (c) R.T. Downs, R.M. Hazen, Chiral indices of crystalline surfaces as a measure of enantioselective potential, J. Mol. Catal. A Chem, 218 (2004) 273–286; (d) R.M. Hazen, Chiral crystal facesof common rock-forming minerals, in: G. Palyi, C. Zucchi, L. Caglioti (Eds.), Progress in Biological Chirality, Elsevier, Oxford, UK, 2004, pp. 137–151; (e) R.M. Hazen, Mineral surfacesand the prebiotic selection and organiztion of biomelecules, Am. Mineral. 93 (2006) 1715–1729; (f) A. Asthagiri, R.M. Hazen, An ab initio study of adsorption of alanine on the chiral calcite (2131) surface, Molec. Simul. 33 (2006) 343–351.

[30] C. Fan, H.H. Teng, Crystallization and dissolution of gypsum, in: D.H. Sampson (Ed.), Gypsum: Properties, Production and Applications, 2011, pp. 111–129. ISBN: 978-1-61728-809-8.

[31] J.M. García-Ruiz, F. Otálora, Crystal growth in geology: patterns on the rocks, in: P. Rudolph (Ed.), Handbook of Crystal Growth, Elsevier, Boston, 2015, pp. 1–43, doi:10.1016/B978-0-444-63303-3.00001-8.

[32] F.R. Massaro, M. Rubbo, D. Aquilano, Theoretical equilibrium morphology of gypsum ($CaSO_4 \cdot 2H_2O$). 2. The stepped faces of the [001] main zone, Crystal Growth Des. 11 (5) (2011) 1607–1614.

[33] W.F. de Jong, J. Bouman, Das reziproke un das Bravaissche Gitter von Gips, Zeit. Krist. 100 (1939) 275–276.

[34] W.F. Cole, C.J. Lancucki, A refinement of the crystal structure of gypsum, ($CaSO_4 \cdot 2H_2O$), Acta Cryst. B30 (1974) 921–929, doi:10.1107/S0567740874004055.

[35] W.M.M. Heijnen, P. Hartman, Structural morphology of gypsum ($CaSO_4{\cdot}2H_2O$), brushite ($CaHPO_4{\cdot}2H_2O$) and pharmacolite ($CaHAsO_4{\cdot}2H_2O$), J. Cryst. Growth 108 (1991) (1991) 290–300.

[36] P. Ramdohr, H. Strunz, F. Enke (Ed.), Klockmanns Lehrbuch der Mineralogie, Stuttgart, 1967.

[37] J.C.A. Boeyens, V.V.H. Icharam, Redetermination of the crystal structure of calcium sulphate dihydrate, $CaSO_4{\cdot}2H_2O$, Zeits. Kristall. 217 (2002) 9–10.

[38] L. Bragg, G.F. Claringbull, W.H. Taylor, Crystal structures of minerals, Cornell University Press, Ithaca, New York, 1965, p. 409.

[39] G.E. Pake, Nuclear resonance absorption in hydrated crystals: fine structure of the proton line, J. Chem. Phys. 16 (4) (1948) 327–336.

[40] B.F. Pedersen, D. Semmingsen, Neutron Diffraction Refinement of the Structure of Gypsum $CaSO_4{\cdot}2H_2O$, Acta Cryst. B38 (1982) 1074–1077.

[41] B. Simon, M. Bienfait, Structure et mécanisme de croissance du gypse, Acta Cryst. 19 (1965) 750–756.

[42] B. Simon, Contribution à l'étude de la formation des macles de croissance, Thèse Univ. d'Aix-Marseille (1968).

[43] E. Van der Voort, P. Hartman, The habit of gypsum and solvent interaction, J. Cryst. Growth 112 (1991) 445–450.

[44] (a) F.R. Massaro, M. Rubbo, D. Aquilano, Theoretical equilibrium morphology of gypsum ($CaSO_4.2H_2O$). 1. A syncretic strategy to calculate the morphology of crystals, Cryst. Growth Des. 10 (7) (2010) 2870–2878, doi:10.1021/cg900660v; (b) F.R. Massaro, M. Rubbo, D. Aquilano, Theoretical equilibrium morphology of gypsum ($CaSO_4.2H_2O$). 2. The stepped faces of the main [001] zone, Cryst. Growth Des. 11 (5) (2011) 1607–1614, doi:10.1021/cg101570c; (c) M. Rubbo, M. Bruno, D. Aquilano, The (102) contact twin of gypsum, Cryst. Growth Des. 11 (6) (2011) 2351–2357, doi:10.1021/cg2000816.

[45] F. Otálora, J.M. García-Ruiz, Nucleation and growth of the Naica giant gypsum crystals, Chem. Soc. Rev. 43 (2014) 2013–2026, doi:10.1039/C3CS60320B.

[46] (a) M.P.C. Weijnen, G.M. van Rosmalen, P. Bennema, J.J.M. Rijpkema, The adsorption of additives on the gypsum crystal surface: I. Determination of the Interfacial bond energies, J. Cryst. Growth 84 (1987) 509–527; (b) M.P.C. Weijnen, G.M. van Rosmalen, P. Bennema, The adsorption of additives on the gypsum crystal surface:a theoretical approach. II. Determina-

tion of the surface coverage required for growth inhibition, J. Cryst. Growth 82 (1987) 528–542.
[47] P. Hartman, W.M.M. Heijnen, Growth mechanism of a crystal face for which more than one surface structure is possible, J. Cryst. Growth 63 (1983) 261–264.
[48] W.M.M. Heijnen, P. Hartman, Structural morphology of gypsum ($CaSO_4.2H_2O$), brushite ($CaHPO_4.2H_2O$) and pharmacolite ($CaHAsO_4.2H_2O$), J. Cryst. Growth 108 (1991) 290–300.
[49] J.M. García-Ruiz, R. Villasuso, C. Aroya, A. Canals, F. Otálora, Formation of natural gypsum megacrystals in Naica, Mexico, Geology 35 (4) (2007) 327–330.
[50] W. Foshag, The selenite caves of Naica, Mexico, Am. Miner. 12 (1927) 252–256.
[51] A.M. Cody, R.D. Cody, Evidence of microbiological induction of {101} Montmartre twinning of gypsum ($CaSO_4.2H_2O$), J. Cryst. Growth 98 (1989a) 721–730.
[52] D. Bosbach, J.L. Junta-Rosso, U. Becker, M.F. Hochella Jr., Gypsum growth in the presence of background electrolytes studied by Scanning Force Microscopy, Geoch. Cosmoch. Acta 60 (17) (1996) 3295–3304.
[53] S. Follner, A. Wolter, K. Helming, C. Silber, H. Bartels, H. Follner, On the real structure of gypsum crystals, Cryst. Res. Technol. 37 (2–3) (2002) 207–218.
[54] M. Rubbo, M. Bruno, F.R. Massaro, D. Aquilano, The five twin laws of gypsum ($CaSO_4.2H_2O$). A theoretical comparison among the interfaces of the contact twins, Cryst. Growth Des. 12 (2012) 264–270, doi:10.1021/cg201031s.
[55] M. Rubbo, M. Bruno, F.R. Massaro, D. Aquilano, The five twin laws of gypsum ($CaSO_4.2H_2O$). A theoretical comparison of the interfaces of the penetration twins, Cryst. Growth Des. 12 (2012) 3018–3024, doi:10.1021/cg300227j.
[56] A.M. Cody, R.D. Cody, SEM and polarization analyzes updating early light microscope studies related to {101} twin formation in gypsum, J. Cryst. Growth 98 (1989b) 731–738.
[57] H. Shindo, M. Kaise, H. Kondoh, C. Nishihara, H. Hayakawa, S. Ono, et al., Structure of cleaved surfaces of gypsum studied with atomic force microscopy, J. Chem. Soc., Chem. Commun. 16 (1991) 1097–1099, doi:10.1039/C39910001097.
[58] D. Bosbach, W. Rammensee, In situ investigation of growth and dissolution on the (010) surface of gypsum by Scanning Force Microscopy, Geoch. Cosmoch. Acta 58 (1994) 843–849.
[59] C. Hall, D.C. Cullen, Scanning force microscopy of gypsum dissolution and crystal growth, Mater. Interfaces Electrochem. Phenom. 41 (1) (1996) 232–238.
[60] D. Bosbach, M.F. Hochella Jr., Gypsum growth in the presence of growth inhibitors: a scanning force microscopy study, Chem. Geol. 1232 (1996) 227–236.
[61] C.F. Fan, H.H. Teng, Surface behavior of gypsum during dissolution, Chem. Geol. 245 (2007) 242–253.
[62] G. Jordan, J.M. Astilleros, In situ HAFM study of the thermal dehydration on gypsum (0 1 0) surfaces, Am. Mineral. 91 (2006) (2006) 619–627.
[63] A.E.S. Van Driessche, J.M. García-Ruiz, J.M. Delgado-López, G. Sazaki, In situ observation of step dynamics on gypsum crystals, Cryst. Growth Des. 10 (9) (2010) 3909–3916.
[64] A.E.S. van Driessche, J.M. García-Ruíz, K. Tsukamoto, L.D. Patiño-Lopez, Ultraslow growth rates of giant gypsum crystals, Proc. Natl. Acad. Sci. U. S. A. 108 (38) (2011) 15721–15726.
[65] K.S. Raju, Evidence of edge and screw dislocations in gypsum single crystals, Bull. Mater. Sci. 2 (2) (1980) 139–144.
[66] C. Rinaudo, M.C. Robert, F. Lefaucheux, Growth and characterization of gypsum crystals, J. Cryst. Growth 71 (1985) 803–806.
[67] G.M. van Rosmalen, P.J. Daudey, W.G.J. Marchée, An analysis of growth experiments of gypsum crystals in suspension, J. Cryst. Growth 52 (1981) 801–811, doi:10.1016/0022-0248(81)90379-1.
[68] M.R. Christoffersen, J. Christoffersen, M. Weijnen, G.M. van Rosmalen, Crystal growth of calcium sulfate dehydrate at low supersaturation, J. Cryst. Growth 58 (3) (1982) 585–595, doi:10.1016/0022-0248(82)90145-2.

## List of selected monographies on the morphology of crystals

Adsorption et Croissance Cristalline", Colloques Intern.Centre Nat. Rech. Sci., n°152, CNRS Ed., 1965, Paris, in French
Crystal Growth: An Introduction", P. Hartman Ed., Nort Holland Series in Crystal Growth, Amsterdam, 1973
Morphology of Crystals, Part A,B,C ", I. Sunagawa Ed., Materials Science of Minerals and Rocks, Terra Sci. Publ. Co. Tokyo, 1987
Morphology and Growth Unit of Crystals", I. Sunagawa Ed., Terra Sci. Publ. Co. Dordrecht, 1989
Surface Morphology of Crystalline Solids", K. Sangwal& R. Rodriguez-Clemente, TransTech Publ., Switzerland, 1991
I. Sunagawa "Growth and Morphology of Crystals" Forma, 14 (1999) 147–166
I. Kostov, R.I. Kostov "Crystal Habits of Minerals", Pensoft Publishers & the Prof. Marin Drinov Academic Publishing House (1999) Bulgarian Acad. Monographs, n°1
H.R. Wenk, A. Bulakh "Minerals: Their Constitution and Origin", Cambridge, 1st edition (2004) ISBN 9780521529587
I. Sunagawa "Crystals–Growth, Morphology and Perfection", Cambridge University Press, Cambridge, U.K. (2005) 308 pp. ISBN-10: 0521841895
F. Abbona, D. Aquilano "Morphology of Crystals Grown from Solutions", Springer Handbook of Crystal Growth, ISBN 978-3-540-74182-4. Springer-Verlag, Berlin, Heidelberg (2010) pp. 53
"Adsorption, Absorption and Crystal Growth", International School, Gargnano (Italy, 2010), D. Aquilano & M. Moret (Eds), a special issue of : Cryst. Res. Technol. 48, n°10, Wiley (2013), 667–941, full text at http://onlinelibrary.wiley.com/doi/10.1002/crat.v48.10/issuetoc
'Crystal Growth in Geology: Patterns on the Rocks' Juan Manuel García-Ruiz and Fermín Otálora", In Handbook of Crystal Growth, edited by Peter Rudolph, Elsevier, Boston, 2015, Pages 1–43, Handbook of Crystal Growth (Second Edition), ISBN 9780444633033, http://dx.doi.org/10.1016/B978-0-444-63303-3.00001-8.